Synthesis of micellar-like terpolymer nanoparticles with reductively-cleavable cross-links and evaluation of efficacy in 2D and 3D models of triple negative breast cancer

Patrícia F. Monteiro[a], Muhammad Gulfam[a], Cíntia J. Monteiro[a], Alessandra Travanut[a], Thais Fedatto Abelha[a], Amanda K. Pearce,[a] Christine Jerôme[b], Anna M. Grabowska[c], Philip A. Clarke[c], Hilary M. Collins[a], David M. Heery[a], Pavel Gershkovich[a] and Cameron Alexander[a]*

[a.]School of Pharmacy, University of Nottingham, NG7 2RD, UK. E-mail: cameron.alexander@nottingham.ac.uk; Tel: +44 (0)115 846 7678.

[b.]Cancer Biology, Division of Cancer and Stem Cells, University of Nottingham, NG7 2UH, UK.

[c.]Center for Education and Research on Macromolecules (CERM), University of Liège, Sart-Tilman, B6, 4000 Liège, Belgium.

KEYWORDS: Triple negative breast cancer, micellar-like nanoparticles, reducible crosslinks, responsive crosslinked nanoparticles, 3D cell culture.

ABSTRACT

Triple negative or basal-like breast cancer (TNBC) is characterised by aggressive progression, lack of standard therapies and poorer overall survival rates for patients. The bad prognosis, high rate of relapse and resistance against anticancer drugs have been associated with a highly abnormal loss of redox control in TNBC cells. Here, we developed docetaxel (DTX)-loaded micellar-like nanoparticles (MLNPs), designed to address the aberrant TNBC biology through the placement of redox responsive cross-links designed into a terpolymer. The MLNPs were derived from poly(ethyleneglycol)-b-poly(lactide)-co-poly(N_3-α-ε-caprolactone) with a disulfide linker pendant from the caprolactone regions in order to cross-link adjacent chains. The terpolymer contained both polylactide and polycaprolactone to provide a balance of accessibility to reductive agents necessary to ensure stability in transit, but rapid micellar breakdown and concomitant drug release, when in breast cancer cells with increased levels of reducing agents. The empty micellar-like nanoparticles did not show any cytotoxicity *in vitro* in 2D monolayers of MDA-MB-231 (triple-negative breast cancer), MCF7 (breast cancer) and MCF10A (normal breast epithelial cell line), whereas DTX-loaded reducible crosslinked MLNPs exhibited higher cytotoxicity against TNBC and breast cancer cells which present high intracellular levels of glutathione. Crosslinked and non-crosslinked MLNPs showed high and concentration-dependent cellular uptake in monolayers and tumour spheroids, including when assessed in co-cultures of TNBC cells and cancer-associated fibroblasts. DTX loaded crosslinked MLNPs showed the highest efficacy against 3D spheroids of TNBC, in addition the MLNPs also induced higher levels of apoptosis, as assessed by annexin V/PI assays and increased caspase 3/7 activity in MDA-MB-231 cells in comparison to cells treated with DTX-loaded un-crosslinked MLNP (used as a control) and free DTX. Taken together these data demonstrate that the terpolymer micellar-like nanoparticles with

reducible crosslinks have high efficacy in both 2D and 3D *in vitro* cancer models by targeting the aberrant biology, i.e. loss of redox control of this type of tumour, thus may be promising and effective carrier systems for future clinical applications in TNBC.

INTRODUCTION

Triple negative breast cancer (TNBC) is a subtype of breast cancer which lacks the expression of estrogen (ER) and progesterone receptors (PR) and also the overexpression of human epidermal growth factor receptor 2 (HER 2), according to the established immunohistochemical profile. It is considered one of the most aggressive types of breast cancer [1-3].

Compared to other types of breast cancer, TNBC patients tend to have a poor prognosis, high recurrence, frequent early visceral metastasis and elevated risk of death [4]. In part, this is due to the difficulty in eradicating TNBC tumours after pre-operative chemotherapy [5]. Unfortunately, patients diagnosed with TNBC cannot take advantage of targeted treatments available for other breast cancer treatments such as hormonal therapy and anti-HER2 agents due to the lack of ER, PR and HE2 receptors [6]. Since there are no standard treatments for TNBC, patients are usually treated with a combination of surgery, radiation and conventional chemotherapy including taxanes and anthracyclines. However, these drugs are associated with various side effects including acute and long-term toxicity, which could contribute to the low overall survival of TNBC patients.[7] Hence, there is an urgent need to develop more targeted treatments for this aggressive type of breast cancer [8].

Due to its aggressiveness and lack of established biomarkers and molecular targets, efforts have been made to elucidate the driving mechanism and also to establish distinct markers that guide in understanding the features of TNBC. Recently, it has been demonstrated that the glutathione

biosynthesis pathway plays a role in the development of TNBC and it is associated with the prevention of cell death and also with poorer patient outcomes. Moreover, one of the causes of high relapse in TNBC patients is the existence and survival of cancer stem cells that are characterised by increased amounts of intracellular glutathione (GSH) levels [9-11]. Thus, it might be possible to exploit the specific and unusual biological features of triple negative breast cancer in order to provide targeted treatments for this highly aggressive subtype of breast cancer [12].

Targeted nanoparticles have the possibility to overcome problems related to chemotherapy by protecting administered drugs from early degradation, reducing toxicity and other side effects, improving intracellular penetration and by providing the drugs with longer circulation half-lives [13, 14]. Further advances for TNBC treatment include the use of stimuli-responsive materials, which can be designed to recognise a particular microenvironment and respond to it by means of a disease-specific local stimulus [15-17].

Many drug delivery systems have been designed to exploit the different concentrations of glutathione (GSH) in the intracellular and extracellular compartments, and in the tumour microenvironment [18]. In addition to the well-known role of GSH as a cellular antioxidant, in the preservation of redox homeostasis, and in the immune response of cells, it is also established that high levels of GSH can also confer resistance to cancer cells against certain chemotherapeutic drugs, contributing to the growth and maintenance of tumours. This has been especially observed in breast, bone marrow, colon, larynx and lung cancers [19-22]. As mentioned above, GSH has been reported as an important therapeutic target in TNBC, thus exploiting the enhanced GSH levels by using redox-responsive nanocarriers to release drugs that are not themselves redox-active, is an appealing route to site-specific TNBC therapies.

These types of materials can be designed by using disulfide bonds that will be cleaved by GSH when the particle enters cancer cells, followed by the release of the drug at a high local concentration for maximum efficacy [23-25]. However, the placement of the disulfide bonds is critical to the function of the nanocarrier, as GSH is a hydrophilic molecule which must be able to access the disulfide linkages in order to affect local drug release. In addition, extracellular reducing species can be present which may act on exposed nanocarrier disulfide linkages to cause non-site-specific drug release, thus there is a trade-off between accessibility and reactivity of disulfide components which must be addressed in any bio-reductively activated drug delivery system [26]. In the present study, we prepared candidate drug-delivery materials of micellar-like nanoparticles (MLNPs) from terpolymers of poly(ethyleneglycol)-poly(lactide)-co-poly(azido)caprolactone (PEG-b-PLA-co-(N_3-PCL)). We also prepared a related terpolymer, but with the poly(lactide) units replaced with unfunctionalised polycaprolactone (PEG-b-PCL-co-(N_3-PCL)). These polymer nanoparticles were subsequently cross-linked by reaction of the azides pendant from the caprolactone units with disulfide-containing bis(alkynes). The chemistries were designed to generate materials with the same reducibly-cleavable functionality, but in one case 'diluted' with polylactide functionality and in the second case with more caprolactone units, with which we aimed to probe the question of disulfide accessibility without 'over-exposure' and the effects of glutathione in breast cancer cells. The interiors of the MLNPs thus varied by having less hydrophobic PLA-co-N_3-PCL units compared to the PCL-co-N_3-PCL components but both had the same outer sterically-stabilising PEG shell [27-29]. In this way, we aimed to evaluate access of GSH into the disulfide-rich regions, ensuring that micelle opening and drug release could only take place once the polymers were installed in regions of abnormally high GSH content, as in TNBC cells (Figure 1). The crosslinking of micellar-based nanomedicines has been successfully

used for addressing the stability issues of this type of delivery system which directly affects their *in vivo* efficacy [30]. Indeed there have been many reducibly-activated crosslinked systems and GSH-responsive approaches which have been designed to increase the *in vivo* efficacy of polymer-mediated drug delivery to tumours [30-32]. In addition, there have been examples of polymer micelles with cores cross-linked via non-cleavable carbon-carbon bond formation, epoxy-amine chemistries, active ester-nucleophile combinations and amide-bond forming reactions to enhance the overall stability of the delivery system in transit *in vivo*. In other cases, reversible cross-links have been formed via polymer carboxylate and platinum complexes,[33] and drug release enhanced by rapidly hydrolysable linkers,[34] thus there are multiple routes by which micellar drug delivery systems can be optimised for a particular therapeutic application.[35] However, many of these systems require complex and laborious organic and/or polymer chemistry methods that can complicate their possible clinical translation. Here we aimed to combine easily accessible copolymer chemistries with the azide-alkyne 1,3-dipolar cycloaddition reaction (*click* chemistry) in order to obtain cross-linked MLNPs in high-yields, with simple reaction conditions, easy purification and less cytotoxic by-products [36, 37]. Therefore, the first target diblock terpolymer was synthesised by ring-opening polymerization of α-chloro-ε-caprolactone and lactide using PEG (polyethylene glycol) as a macroinitiator. The chloro groups of the polymer were then replaced by azide groups to obtain mPEG-b-poly(D,L-lactide-co-α-N_3-ε-caprolactone). The second diblock terpolymer of mPEG-b-poly(caprolactone)-co-α-N_3-ε-caprolactone) was prepared by a similar method [38]. Crosslinked MLNPs were subsequently prepared through the use of a bis-alkyne crosslinker, which was attached to the polymer by standard azide-alkyne coupling, leading to self-assembly of the polymer chains into stabilised micellar-like nanoparticles. The resultant materials were characterised by dynamic light scattering (DLS), zeta potential measurements and

transmission electron microscopy (TEM). High pressure liquid chromatography (HPLC) was used for evaluating drug-loading capacities and *in vitro* drug release.

We compared the effectiveness and cytotoxicity of the DTX-loaded crosslinked and un-crosslinked MLNPs and free DTX against triple negative breast cancer cells (MDA-MB-231). The un-crosslinked formulation was used as a control for the experiments. Cytotoxicity of the empty MLNPs was also evaluated by MTS assays in MDA-MB-231, MCF7 (breast cancer cells), and in MCF10A cells, which are from a non-cancerous human breast epithelial cell line. The internalisation of Cy5-labelled MLNPs in monolayers and tumour spheroids of MDA-MB-231 and co-culture with cancer-associate fibroblasts was evaluated using flow cytometry and confocal microscopy, and the capability of the DTX-loaded crosslinked, un-crosslinked MLNPs and free DTX to induce apoptosis in MDA-MB-231 cells was studied by using the annexin-V/PI assay. The activation of caspase-3/7 was also assessed in the same TNBC cell line after treatment with DTX-loaded MLNPs and free drug. DTX-loaded crosslinked MLNPs also had a superior effectiveness against 3D spheroids of TNBC in comparison to the other un-crosslinked formulation and free drug which was assessed by calcein-AM and ethidium homodimer double staining for distinguishing in between live and dead cells. Overall, these *in vitro* experiments in 2D and 3D indicated that crosslinked reductive MLNPs had an increased uptake and selective enhanced efficacy on breast cancer cells presenting higher intracellular levels of GSH, including TNBC cells.

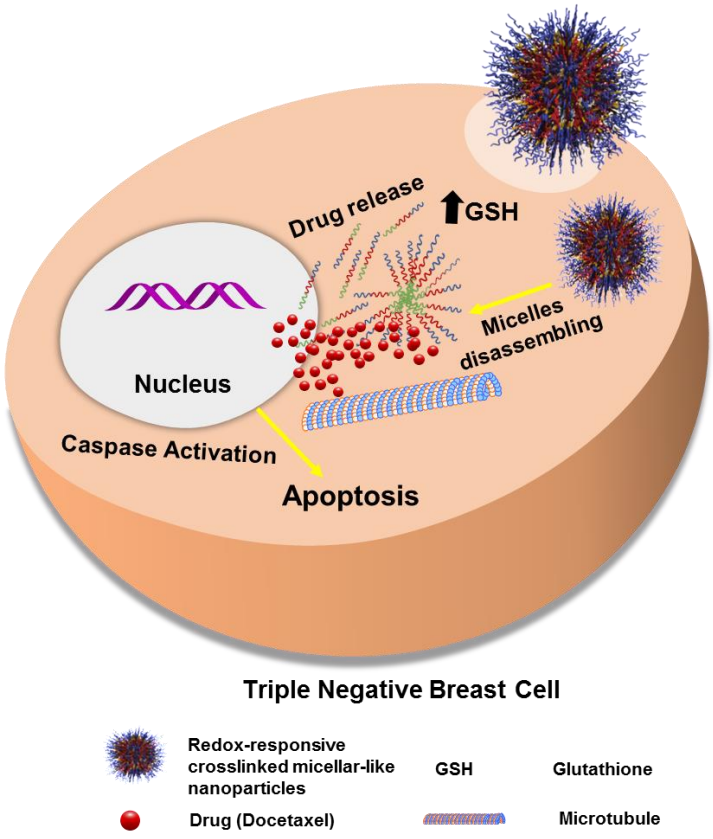

Figure 1 Outline illustration of DTX-loaded redox-responsive crosslinked micellar-like nanoparticles inducing apoptosis in the triple negative breast cancer cell.

EXPERIMENTAL SECTION

Materials and Methods

Docetaxel (European Pharmacopoeia standard), 2-chlorocyclohexanone (98%), 3-chloroperoxybenzoic acid (mCPBA, 70%), monomethoxy poly(ethylene glycol) (mPEG, Mn-5000 g/mol), tin(II) 2-ethylhexanoate ($Sn(Oct)_2$), (92.5-100%) sodium azide (≥99.5%), propargylamine (98%), copper (II) sulfate (99.9%), ascorbic acid sodium salt (≥98%), 2-hydroxyethyl disulfide (90%), N-(3-dimethylaminopropyl)-N′-ethylcarbodiimide hydrochloride (EDAC, 99%), 4-pentynoic acid (95%), ethylenediaminetetraacetic acid (EDTA, 99.4-100%) and

deuterated chloroform ($CDCl_3$) were all purchased from Sigma-Aldrich. Cyanine5 (Cy5) alkyne fluorescent dye was purchased from Lumiprobe. All solvents were purchased from Fisher Scientific. Propidium iodide (PI), Hoechst 33342, CellMask™ Green plasma membrane stain, Dead cell apoptosis kit Annexin-V/PI, CellEvent™ Caspase-3/7 Green and LIVE/DEAD® Viability/Cytotoxicity Assay Kit were purchased from Thermo Fisher Scientific. CellTiter 96® Aqueous One solution of MTS was purchase from Promega. Ultra-low attachment 96-well round bottom (black and clear) plates were purchased from Corning Incorporated Life Sciences, USA. All chemicals were used as received unless otherwise stated.

Monomer and polymer syntheses

Synthesis of α-chloro-ε-caprolactone monomer

The monomer α-chloro-ε-caprolactone was synthesised using a method previously described [39]. Briefly, at room temperature, 10 g (40.5 mmol) of mCPBA (70%) was transferred to a flask containing a solution of 2-chlorocyclohexanone (5 g, 37.5 mmol) in 50 mL of dichloromethane. The reaction was left to run for 96 h and afterwards, the obtained product was cooled to -20ºC to crystallize the unreacted m-chlorobenzoic acid. The compound was filtered and washed three times with saturated solutions of $Na_2S_2O_3$/ NaCl and $NaHCO_3$. Finally, the organic layer was washed with water and dried over $MgSO_4$. Subsequently, the organic phase was filtered and then concentrated using a rotary evaporator to obtain a yellow viscous liquid which was purified by silica gel flash column chromatography (hexane: ethyl acetate 9:2, Rf 0.36). The yield of the α-chloro-ε-caprolactone obtained was 3.50 g (70%). ^{1}H NMR (400 MHz, $CDCl_3$, δ in ppm): 4.85-4.81 (s, 1H), 4.69-4.63 (m, 1H), 4.29-4.23 (m, 1H), 2.23-1.77 (m, 6H). All the characterisation data were in accord with prior literature reports for this compound [39].

Synthesis of mPEG-b-poly(D,L-lactide-co-α-Cl-ε-caprolactone)

The copolymer was synthesised by ROP (ring-opening polymerisation) of α-chloro-ε-caprolactone and D,L-lactide using $mPEG_{5000}$ as a macroinitiator and $Sn(Oct)_2$ (tin-II ethylexanoate) as a catalyst. D,L-lactide (1.00 g) and chloro-ε-caprolactone (1.03 g) were transferred into a flask containing $mPEG_{5000}$ (5.00 g) which was previously dried by azeotropic distillation with anhydrous toluene. The contents were heated at 90°C and solubilized with 10 mL of anhydrous toluene added into the sealed flask under nitrogen atmosphere. At this moment, $Sn(Oct)_2$ (0.002 g) was added and the reaction was left to proceed at 90°C for 24 h under stirring. Afterwards, the reaction was cooled to room temperature. The product was dissolved in dichloromethane and precipitated in diethyl ether. It was then filtered and dried under reduced pressure until constant weight was achieved. A white powder was obtained in a 75% yield. ^1H NMR (400 MHz, $CDCl_3$, δ in ppm): δ 5.20 (d, J = 6.0 Hz, 5H), 4.28 (dd, J = 37.1, 17.4 Hz, 10H), 3.67 (s, 320H), 3.41 (s, 2), 2.07 (d, J = 40.1 Hz, 7H), 1.67 – 1.41 (m, 35H).

Synthesis of mPEG-b-poly(D,L-lactide-co-α-N_3-ε-caprolactone)

The azide-functionalised copolymer was obtained through a substitution reaction between chloro and azide groups. Typically, mPEG-*b*-poly(D,L-lactide-*co*-α-Cl-ε-caprolactone) (1.00 g) was transferred into a flask and dissolved in 3 mL of DMSO (dimethyl sulfoxide). Subsequently, sodium azide (0.088 g) was carefully added and the reaction was allowed to proceed for 24 h at room temperature. The product was dissolved in a small amount of dichloromethane and extracted with diethyl ether to remove DMSO before filtering. The reaction product was then dissolved in toluene and centrifuged in order to remove the insoluble salts followed by the precipitation of the polymer in diethyl ether. The obtained functionalised copolymer was filtered and dried under reduced pressure until constant weight was achieved. A pale yellow powder was obtained in a

yield of 0.80 g, (80%). ^{1}H NMR (400 MHz, $CDCl_3$, δ in ppm): δ 5.37 – 5.08 (m, 2H), 4.45 – 4.08 (m, 2H), 3.67 (s, 133H), 3.40 (s, 1H), 1.70 (d, J = 31.0 Hz, 11H), 1.67 – 1.40 (m, 10H).

Synthesis of Cy5-labelled mPEG-b-poly(D,L-lactide-co-α-N_3-ε-caprolactone)

Briefly, 110 mg (0.016 mmol) of the copolymer and 10 mg (0.0179 mmol) of Cy5-alkyne were added into a flask and dissolved in 2 mL of DMSO. A 265 µL of an ascorbic acid solution 25 mg/mL was added and the reaction was purged with nitrogen and left stirring. Afterwards, 520 µL of copper (II) sulfate solution (10 mg/mL) was added into the flask and the reaction was allowed to stir overnight at room temperature. EDTA was added (19.04 mg, 0.065 mmol / 2 eq vs. Cu) and the polymer was purified by dialysis in order to remove any unreacted dye. Subsequently, the labelled polymer was frozen and lyophilised. The conjugation efficiency was determined by fluorescence spectroscopy.

Synthesis of bis-alkyne ethyl disulfide crosslinker (disulfanediylbis(ethane-2,1-diyl) bis(pent-4-ynoate)

Disulfanediylbis(ethane-2,1-diyl) bis(pent-4-ynoate) was synthesised by adding 1.31 g (8.49 mmol) of 2-hydroxyethyl disulfide, 3.90 g (20.34 mmol) of *N*-(3-dimethylaminopropyl)-*N'*-ethylcarbodiimide hydrochloride (EDAC), and 4-pentynoic acid (2 g, 20.38 mmol) into a flask containing anhydrous dichloromethane at 0^{o}C. Afterwards, 4-(dimethylamino) pyridine (0.25 g, 2.05 mmol) was dissolved in dichloromethane and then was added under stirring and the mixture was left to react for 48 h at room temperature. The purification of the bis-alkyne crosslinker was carried out by washing the reaction product with the followed solutions: 1M hydrochloric acid (3 x 100 mL), 1M sodium hydroxide (3 x 100 mL) and 1M NaCl (200 mL). The mixture was then dried over $MgSO_4$ and the solvent was removed under reduced pressure. Finally, the crude product

was purified by flash column chromatography (hexane: ethyl acetate 4:3) yielding 0.98 g, (75%). ^{1}H NMR (400 MHz, $CDCl_3$, δ in ppm): 4.39 (t, 4 H), 2.95 (t, 4H), 2.63 – 2.57 (m, 4H), 2.56 – 2.50 (m, 4H), 2.01 (t, 2H). The characterisation data were in accord with prior literature reports for this compound [40].

Preparation of empty and docetaxel or Cy5-labelled un-crosslinked micellar-like nanoparticles

In this work, all the micellar formulations were prepared by a dialysis method, using dimethyl sulfoxide as the organic solvent inside the dialysis membrane, and water as the bulk phase. In a typical experiment, empty MLNPs were prepared by dissolving 12.5 mg of the mPEG-b-poly(D,L-lactide-co-α-N_3-ε-caprolactone) copolymer in 2 mL of dimethyl sulfoxide. The solution was added to 10 mL of ultrapure water, while stirring, using a syringe pump (flow rate: 0.1 mL/min). Afterwards, the obtained solution was transferred into a dialysis membrane (cut-off 3500 Da) and was left dialysing against water for 24 h. DTX-loaded MLNPs were prepared by using 2 mg of DTX and 12.5 mg of the copolymer. The method of preparation was similar as described for empty MLNPs. Cy5-labelled un-crosslinked MLNPs were prepared as described above, however the particles were prepared by using a 50:50 w/w mixture of Cy5-labelled polymer and unlabelled polymer. The obtained micellar suspensions were then filtered through a syringe membrane filter before further analysis (0.22 μm) (Millex-LG, Millipore Co., USA). The particle size (z-average diameter) and zeta potential of all prepared micelles were measured using NanoZS equipment (Malvern, UK) at 25^{o}C. Morphology of MLNPs was analysed by transmission electron microscopy using a Tecnai G2 (FEI, Oregon, USA). Images were obtained without staining.

Preparation of empty and docetaxel or Cy5-labelled crosslinked micellar-like nanoparticles

Empty crosslinked MLNPs were prepared by dissolving 12.5 mg of the mPEG-*b*-poly(D,L-lactide-*co*-α-N_3-ε-caprolactone) and 4.9 mg (0.01 mmol) of bis-alkyne ethyl disulfide crosslinker in 2 mL of dimethyl sulfoxide and the mixture was allowed to stir for 2 hours. Afterwards, the solution was added dropwise to 10 mL of ultrapure water using a syringe pump (flow rate: 0.1 ml/min) and then copper(II) sulfate (0.5 mg, 0.003 mmol) and ascorbic acid sodium salt (0.6 mg, 0.003 mmol) were added. The reaction was run for 24 h at 36ºC. Before dialysing the obtained product against water (cut-off 3500 Da), EDTA was added (13.03 mg, 0.044 mmol / 2 eq vs. Cu). The preparation method for DTX-loaded MLNPs was similar to the method described above in which 2 mg of DTX was used for 12.5 mg of copolymer. Cy5-labelled crosslinked MLNPs were prepared as described above, however the particles were prepared by using a 50:50 w/w mixture of Cy5-labelled polymer and unlabelled polymer. The methods used to characterise crosslinked MLNPs were similar to those described for un-crosslinked MLNPs. In order to assess responsiveness to redox environments, empty crosslinked MLNPs were treated with 10 mmolar GSH solution in PBS for 4 h and the differences in the morphology and size were observed by checking samples by DLS and TEM (Figure 3).

Drug content and encapsulation efficiency

The quantification of DTX in the MLNPs was determined using a HPLC-DAD (Shimadzu, Prominence, Japan) quantification method. The HPLC system was equipped with a photodiode array (PDA) detector and autosampler. LC solution software was used to analyse the chromatograms. A Phenomenex Aeris C18 column at room temperature (150 x 4.6 mm, 3.6 µm) was used and the mobile phase consisted of water: acetonitrile (60:40) at a flow rate of 0.7 mL/min. The method was previously validated for specificity, linearity, accuracy and precision. In short, 1

mg of MLNPs were dissolved and sonicated in 5 mL of acetonitrile, after which the solution was filtered and transferred to the vial for quantification. The analysis was performed in triplicate. The injection volume was 10 μL and DTX was detected at 224 nm. The encapsulation efficiency was expressed as the percentage of drug loaded into the MLNPs (Table 1).

In vitro drug release study

The release rate of DTX from the crosslinked MLNPs was measured in a reductive (10 mM of GSH in PBS) and non-reductive (PBS without GSH) media. The non-reductive media was used as a control for the experiment. The DTX released from the un-crosslinked MLNPs was also measured in PBS without GSH. In all the three samples prepared, 0.1% of tween 20 (polysorbate 20) was added to help with the solubilisation of DTX. Briefly, 3 mg of freeze-dried crosslinked and un-crosslinked MLNPs were dissolved in 0.8 mL of PBS (0.1% tween 20) and the solution was placed in a dialysis device (Slide-A-Lyzer, Thermo Scientific). The DXT-loaded MLNPs were left dialysing against 2 mL of the mentioned release media in a shaking water bath at 37^{o}C. Aliquots of 200 μL were taken at each time point and the collected samples were replaced with the same volume of fresh media to maintain sink conditions. The amount of DTX present in each aliquot was analysed by HPLC using the same method and conditions shown in 'Drug content and encapsulation efficiency'. The cumulative release (%) was defined based on the concentration of DTX calculated in the samples collected at different time points and considering the initial amount of encapsulated drug into the MLNPs.

Cell lines, culture and development of 3D tumour spheroids model

Breast cancer MCF7, triple negative breast cancer cell line MDA-MB-231 and the non-cancerous human mammary epithelial cells MCF10A were acquired from the American Type Culture Collection (Manassas, VA). Cancer-associated fibroblasts (CAFs) were obtained as previously shown [41]. In brief, samples of fresh surgical materials from tumour resections at Nottingham University Hospitals NHS Trust were used after being approved the appropriate Research Ethics Committees as shown elsewhere [41]. Samples were then dissected and fixed for immunohistochemistry. Afterwards, an amount of minced tumour tissue was disaggregated and cultured in DMEM, 10% FBS, 2 mmol/L glucose for the establishment of fibroblasts. The identity of CAFs was confirmed by appropriate methods [41]. The cancer cell lines were maintained in Dulbecco's modified Eagle's medium (DMEM, Lonza, Inc), supplemented with 10% (v/v) FBS and 1% penicillin/ streptomycin and incubated at 37ºC in 5% CO_2. MCF10A was maintained in human mammary epithelial cell growth complete medium which consisted of HuMEC basal serum free medium with HuMEC supplemented kit (HuMEC Ready Medium, Gibco).

TNBC tumour spheroids were obtained using ultra-low attachment (ULA) 96-well round bottom plates (Corning, UK). MDA-MB-231 cells were seeded into ULA plates at a density of 4000 per well and cells were centrifuged at 300 x g for 3 minutes after seeding to bring the cells closer together and aid in the formation of a single spheroid. Spheroids were then cultured for 3 days before final analysis or treatment.

For the 3D co-culture, MDA-MB-231 and GFP-transfected CAFs were seeded in ULA plates at a density of 2000:2000 cells per well and the method for obtaining the spheroids was similar to the previously described.

Cell proliferation analysis

The cytotoxicity of the empty and DTX-loaded crosslinked and un-crosslinked MLNPs was assessed by the MTS 3-(4,5-dimethyl-2-yl)-5-(3-carboxymethoxyphenyl)-2-(4-sulfophenyl)-2H-tetrazolium (CellTiter 96® AQ_{ueous} One Solution Reagent, Promega) assay. MDA-MB-231, MCF7 or MCF10A cells were seeded into a 96 well-plate at a density of 5 x 10^3 cells per well and incubated at 37ºC and 5% of CO_2 for 24 h. Afterwards, cells were exposed to different concentrations of empty MLNPs (100, 250, 500, 750 and 1000 μg/mL) and DTX-loaded MLNPs (7-40 μg/mL of DTX) for 24 hours. Controls containing only medium and DMSO were also prepared. MLNPs were diluted using complete medium. After the incubation time, 20 μg/mL of MTS solution was added in each well and then cells were left incubating for an additional 3 hours. Absorbance was measured using a BioTek microplate reader at 490 nm. Experiments were made in replicates and repeated in different days and the percentage of metabolic activity (mean % ± SD) was reported compared to the control. For all experiments both technical and biological replicates were performed.

Cell uptake studies

Cellular uptake in 2D and 3D cell culture

2D monolayers of TNBC cells assessed by confocal microscopy

Human triple negative breast cancer monolayers of MDA-MB-231 cells were cultured on micro slide 8-well chambers (Ibidi, Germany) at a density of 1 x 10^4 cells per well for 24 h in DMEM complete medium (Lonza, Inc) at 37ºC in 5% CO_2 for 24 h. Cells were then exposed to Cy5-labelled crosslinked and un-crosslinked MLNPs at concentrations of 50 μg/mL in the dark for 4 hours. Following incubation, cells were washed with PBS (phosphate-buffered saline) for three times and then fixed with 4% formaldehyde (in PBS) for 10 min and again washed with PBS (3

times). Afterwards, cells were exposed to Deep Green plasma membrane staining at the concentration of 1 µL/mL (100 µL) for 10 minutes in the dark at 37°C and washed with PBS for 3 times. Cells were then incubated with Hoechst 33342 dye at concentration of 1 µL/mL (100 µL) for 30 minutes in the dark at room temperature and washed again with PBS (three times). Cells were imaged with a Zeiss LSM 510 Meta confocal microscope and Zeiss LSM software was used for data analyses.

2D monolayers of TNBC cells assessed by flow cytometry

MDA-MB-231 cells were cultured on 6-well plates at a density of 7.5 x 10^4 cells per well for 24 h in DMEM complete medium (Lonza, Inc) at 37ºC in 5% CO_2. Cell culture medium was replaced with the medium containing Cy5-labelled crosslinked or un-crosslinked MLNPs at concentrations of 10, 25, 50, 100 and 150 µg/mL and cells were incubated for 4 h at 37ºC in 5% CO_2. Medium was then removed and cells were washed with PBS 3 times and then detached with 500 µL of 1x trypsin/EDTA solution. Cells were centrifuged and resuspended in 500 µL of paraformaldehyde solution in PBS (4%) and then analysed by flow cytometry (Beckman Coulter FC 500). Generated data were analysed using Kaluza 1.5 software.

Uptake in 3D tumour spheroids

Confocal microscopy

MDA-MB-231 cells were seeded into a ULA 96 well-plate at a density of 4000 per well and the spheroids were formed using the same procedure as shown previously. The spheroids were then exposed to 50 µg/mL of Cy5-labelled crosslinked and un-crosslinked MLNPs and they were incubated for 5 h at 37°C in 5% CO_2. Afterwards, the media was gradually removed and the spheroids were carefully washed with PBS 3 times. The spheroids were fixed with 4%

formaldehyde (in PBS) for 10 min and again washed with PBS (3 times). The spheroids were then stained with Hoechst 33342 dye at concentration of 1 μg/mL (50 μL) for 30 minutes in the dark at room temperature and washed again with PBS (three times). Cells were imaged with a Leica TCS microscope. Images were processed using LASX software and ImageJ.

3D co-culture spheroids were obtained by seeding MDA-MB-231 and CAFs in the proportion of 2000:2000 cells per well. The spheroids were obtained and treated and prepared for imaging using the same procedure previously described. Spheroids were imaged with a Zeiss LSM 880 and images were processed using Zen 2 (blue edition).

Flow Cytometry

3D spheroids as monoculture (MDA-MB-231 cells) and co-culture (MDA-MB-231 and CAFs) were prepared as previously described and treated with 50 μg/mL and 150 μg/mL of Cy5-labelled crosslinked and un-crosslinked MLNPs and incubated for 5 h. After the incubation period, the spheroids were carefully dissociated using TrypLE™ Express Enzyme (1X). The resultant single cell suspensions from nineteen wells per condition/ treatment were pooled together in a microcentrifuge tube and cells were centrifuged and washed with PBS 3 times. Samples were analysed using a Beckman Coulter FC 500 flow cytometer. Kaluza 1.5 software was used for the data analysis.

Apoptosis assays in 2D monolayers of TNBC

Annexin-V/ PI

MDA-MB-231 cells were cultured on 6-well plates at a density of 7.5 x 10^4 cells per well for 24 h in DMEM complete medium (Lonza, Inc) at 37ºC in 5% CO_2. Cell culture medium was replaced with the medium containing free DTX, DTX-loaded crosslinked or un-crosslinked MLNPs at the concentration of 7 μg/mL (of DTX) or medium in the absence of MLNPs (controls) and cells were

incubated for 24 h at 37ºC in 5% CO_2. After the incubation period, supernatants were collected and then adhered cells were detached with 500 µL of 1x trypsin/EDTA solution. Cells were centrifuged and washed with PBS. Afterwards, cells were resuspended in 100 µL of 1X annexin-binding buffer and 2.5 µL annexin-V FITC (Thermo Scientific) and 1 µL of 100 µg/mL PI solutions were added. The negative control sample cells were left untreated and unstained, while the other two control samples were also left untreated, but the cells were stained with annexin-V and PI, respectively. Cells were incubated in the dark for 15 min and then 400 µL of 1X annexin-binding buffer was added. Samples were immediately analysed using a Beckman Coulter FC 500 flow cytometer. Kaluza 1.5 software was used for the data analysis as before.

Detection of caspase-3/7

As previously described for annexin-V/PI assay, MDA-MB-231 cells were cultured on 6-well plates at a density of 7.5 x 10^4 cells per well for 24 h in DMEM complete medium (Lonza, Inc) at 37ºC in 5% CO_2. Cell culture medium was then replaced with the medium containing DTX-loaded crosslinked and un-crosslinked MLNPs or free drug at the concentration of 7 µg/mL (of DTX) and controls (untreated cells) were also prepared. After the incubation period (24 h at 37ºC in 5% CO_2), supernatants were collected and adhered cells were detached with 500 µL of 1x trypsin/EDTA solution for 3 minutes. Cells were washed with PBS, resuspended, and then transferred to the FACS tubes. CellEvent™ Caspase-3/7 Green Detection reagent at the concentration of 500 µM was added to the tubes (1 µL) and cells were incubated for 30 minutes at 37ºC protected from light. After 25 minutes of incubation, 1 µL SYTOX™ AADvanced red at a concentration of 1 mM was added and cells were incubated for a further 5 minutes at 37ºC. Samples were then analysed without washing or fixing using a Beckman Coulter FC 500 flow cytometer and data were analysed using Kaluza 1.5 software.

Live/Dead cell staining of TNBC 3D spheroids

MDA-MB-231 cells were seeded into a ULA 96 well-plate at a density of 4000 per well and the spheroids were formed using the same procedure as shown previously. Cell culture medium was replaced with the medium containing free DTX, DTX-loaded crosslinked or un-crosslinked MLNPs at the concentration of 7 μg/mL (of DTX) or medium in the absence of MLNPs (negative control) or 12% of DMSO (positive control) and cells were incubated for 24 h at 37ºC in 5% CO_2. Afterwards, the media was gradually removed and the spheroids were carefully washed with PBS. The spheroids were then stained with 2 μM of calcein AM and 4 μM of EhD-1 solution in PBS and incubated for 1 h at room temperature and washed again with PBS (three times). The spheroids were fixed with 4% formaldehyde (in PBS) for 10 min and again washed with PBS (3 times). Cells were imaged with a Zeiss 710 confocal microscope. Images were processed using Zeiss Zen microscope software. For performing the quantitative live/dead cell assay the experiment were performed as shown however, spheroids were disintegrated using TrypLE™ Express Enzyme (1X) and cell were analysed using a plate reader. As before, technical and biological replicates were performed.

Statistical analysis

Statistical significances were determined using t-test or analysis of variance (one-way and two-way ANOVA). Values of $p < 0.05$ were considered statistically significant.

RESULTS AND DISCUSSION

Synthesis, characterisation and functionalisation of monomer and polymers

The α-chloro-ε-caprolactone monomer was synthesised by a Baeyer-Villiger reaction as shown in Figure 2A. Oxidation was performed by 3-chloroperoxybenzoic acid (mCPBA) to convert α-chlorocyclohexanone to α-chloro-ε-caprolactone and ε-chloro-ε-caprolactone in a molar ratio of 95/5. The crude product was purified by flash column chromatography on silica gel in order to obtain the desired monomer, as indicated in the ^{1}H NMR spectrum of the purified product (Figure S1). The characterisation data for the obtained compound were in agreement with the reported literature data for α-chloro-ε-caprolactone using the same synthetic route [39].

The novel copolymer mPEG-b-poly(D,L-lactide-*co*-α-Cl-ε-caprolactone) was synthesised via ring-opening polymerization of α-chloro-ε-caprolactone and the D,L-lactide using $mPEG_{5000}$ as macroinitiator and $Sn(Oct)_2$ as a catalyst (Figure 2B). The polymer was characterised by ^{1}H NMR and ^{13}C NMR as shown in Figures S2 and S3. The M_n of the polymer as determined by ^{1}H NMR was 7100 g mol^{-1}, whereas the molar mass obtained from the SEC (size exclusion chromatography) (Figure S4) was 11680 g mol^{-1}. Polymer mPEG-*b*-poly(D,L-lactide-*co*-α-Cl-ε-caprolactone) afforded a narrow molecular weight distribution (1.03) of M_w/M_n at room temperature, according to SEC traces of the polymer. Subsequently, the chloro substituents of the mPEG-*b*-poly(D,L-lactide-*co*-α-Cl-ε-caprolactone) polymer were replaced via nucleophilic substitution reactions using sodium azide in order to obtain an azide functionalised copolymer (mPEG-*b*- poly(D,L-lactide-*co*-α-N_3-ε-caprolactone), as shown in Figure 2C. The reaction was performed in mild conditions, e.g. room temperature and using DMSO as the solvent, in order to avoid side reactions and formation of by-products. The functionalised polymer was characterised by ^{1}H NMR, ^{13}C NMR and Fourier transform infrared spectroscopy (FT-IR) (Figure S5, S6 and S7). As can be noticed in Figure S7, the FT-IR spectrum of mPEG-*b*-poly(D,L-lactide-*co*-α-N_3-ε-caprolactone) indicates the characteristic azide peak at ~ 2100 cm^{-1}. The absence of any new carboxylate or OH

bands demonstrated that the polymer did not suffer any degradation during the chloro-to-azide substitution reaction. Cy5-labelled mPEG-*b*-poly(D,L-lactide-*co*-α-N_3-ε-caprolactone) polymer was obtained through CuAAC (copper catalysed azide- alkyne 1,3-dipolar cycloaddition) reaction between the azide groups at the polymer backbone and the alkyne group present in the Cy5-alkyne dye (Scheme S1). The conjugation efficiency results determined by fluorescence spectroscopy showed that there were 1-1.5 Cy5 units per polymer chain. FT-IR was also used to monitor the conjugation of Cy5 to the polymer. As shown in Figure S8 there was a decrease of the azide peak of the labelled polymer at ~ 2100 cm^{-1} after the conjugation reaction in comparison to the non-labelled azide functionalised polymer.

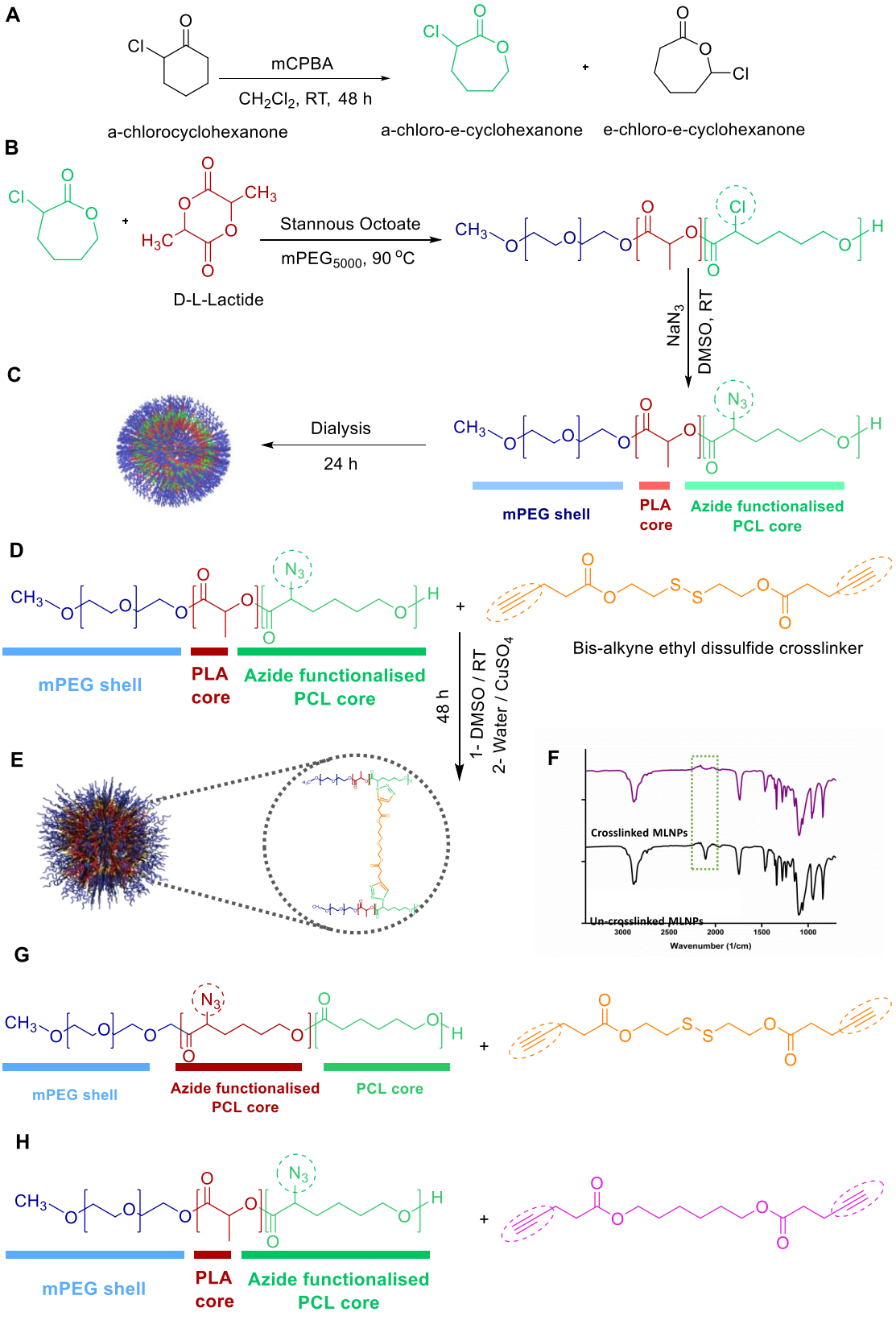
A
mCPBA
CH_2Cl_2, RT, 48 h
a-chlorocyclohexanone
a-chloro-e-cyclohexanone
e-chloro-e-cyclohexanone
B
D-L-Lactide
Stannous Octoate
$mPEG_{5000}$, 90 °C
NaN_3
DMSO, RT
C
Dialysis
24 h
mPEG shell
PLA core
Azide functionalised PCL core
D
mPEG shell
PLA core
Azide functionalised PCL core
Bis-alkyne ethyl dissulfide crosslinker
48 h
1- DMSO / RT
2- Water / $CuSO_4$
E
F
Crosslinked MLNPs
Un-crosslinked MLNPs
Wavenumber (1/cm)
G
mPEG shell
Azide functionalised PCL core
PCL core
H
mPEG shell
PLA core
Azide functionalised PCL core

Figure 2 (A) Schematic representation of the reaction to obtain α-chloro-ε-caprolactone. (B) Synthesis of mPEG-*b*-poly(D,L-lactide-*co*-α-Cl-ε-caprolactone) and mPEG-*b*-poly(D,L-lactide-*co*-α-N_3-ε-caprolactone). (C) Self-assembly of un-crosslinked MLNPs. (D) Preparation of redox responsive core crosslinked MLNPs by alkyne-azide cycloaddition reaction between mPEG-*b*-poly(D,L,lactide-*co*-α-N_3-ε-caprolactone) and crosslinker molecule and dialysis method (E) Self-assembly of crosslinked MLNPs by dialysis method. (F) FT-IR of freeze dried MLNPs showing the absence of azide peak at about 2100 cm^{-1} in the crosslinked MLNPs (shown on purple line). (G) Preparation of comparator redox responsive core crosslinked MLNPs control through a reaction between mPEG-b-poly(ε-caprolactone-co-α-N_3-ε-caprolactone) and the responsive crosslinker. The reaction and micellization was obtained using the alkyne-azide cycloaddition similarly as shown in Figure 2D. (H) Preparation of non-responsive core crosslinked MLNPs control using a non-responsive linker. The reaction and formulation were prepared as shown in Figure 2D above.

Preparation and characterisation of crosslinked and un-crosslinked MLNPs

In this work, a dialysis method was used to prepare both crosslinked and un-crosslinked micellar formulations. The un-crosslinked MLNPs were formed from the self-assembly of mPEG-*b*-poly(D,L-lactide-*co*-α-N_3-ε-caprolactone) in water, as shown in Figure 2C.

Crosslinked MLNPs were prepared firstly by the copper catalysed cycloaddition reaction between azide groups of the polymer and the alkynes from the synthesised crosslinker, as shown in Figure 2D. The bis-alkyne crosslinker was previously synthesised from 2-hydroxyethyl disulfide and propargylacetic acid using DMAP and EDC as catalyst and activating agent, respectively and was characterised by ^{1}H NMR and ^{13}C NMR (Figure S9 and S10). At the end of the micellar core cross-linking reaction, copper sulphate was removed using EDTA to leave self-assembled nanoparticles crosslinked by 1,2,3-triazole linkages, as shown in Figure 2E.

FT-IR was used to monitor the cycloaddition reaction and the formation of core-crosslinked MLNPs (Figure 2F) which resulted in the disappearance of the azide band in comparison to the un-crosslinked freeze dried MLNPs [42].

The scheme with the chemical structures used for preparing the mPEG-b-poly(ε-caprolactone-co-α-N_3-ε-caprolactone) crosslinked MLNPs and the non-responsive crosslinked MLNP are shown in Figure 2E-H. The characterisation of the polymers and MLNPs and the results before and after treatment with GSH are shown in Figure S15-S19 in the supplementary information.

Characterisation data from the crosslinked and un-crosslinked MLNPs are presented in Figure 3 and Table 1. The size distributions (hydrodynamic diameter) and zeta potentials were measured by light scattering. The morphology of the MLNPs was determined by TEM. The size of the empty un-crosslinked MLNPs was 31 nm ± 1, whereas for the crosslinked MLNPs the size was 41 nm ± 0.5. The larger hydrodynamic diameter of the crosslinked MLNPs was expected, as there were likely to be conformational changes regarding the formation of the triazole ring and enhanced rigidity in the micellar cores [40].

MLNPs loaded with DTX were also increased in size, as expected. TEM images presented in Figure 3C show that both types of MLNPs presented with spherical morphologies. These data suggested that both micellar formulations might be suitable for drug delivery in cancer therapy, as it has been reported that nanomedicines in the sub-100 nm range have increased penetration and accumulation in tumours [43, 44]. More importantly, it was demonstrated that MLNPs in the 30 – 50 nm size range showed superior accumulation in tumours, including those of lower permeabilities [45]. Thus, the formulations prepared were deemed suitable in terms of size to be taken forward for *in vitro* and *in vivo* studies.

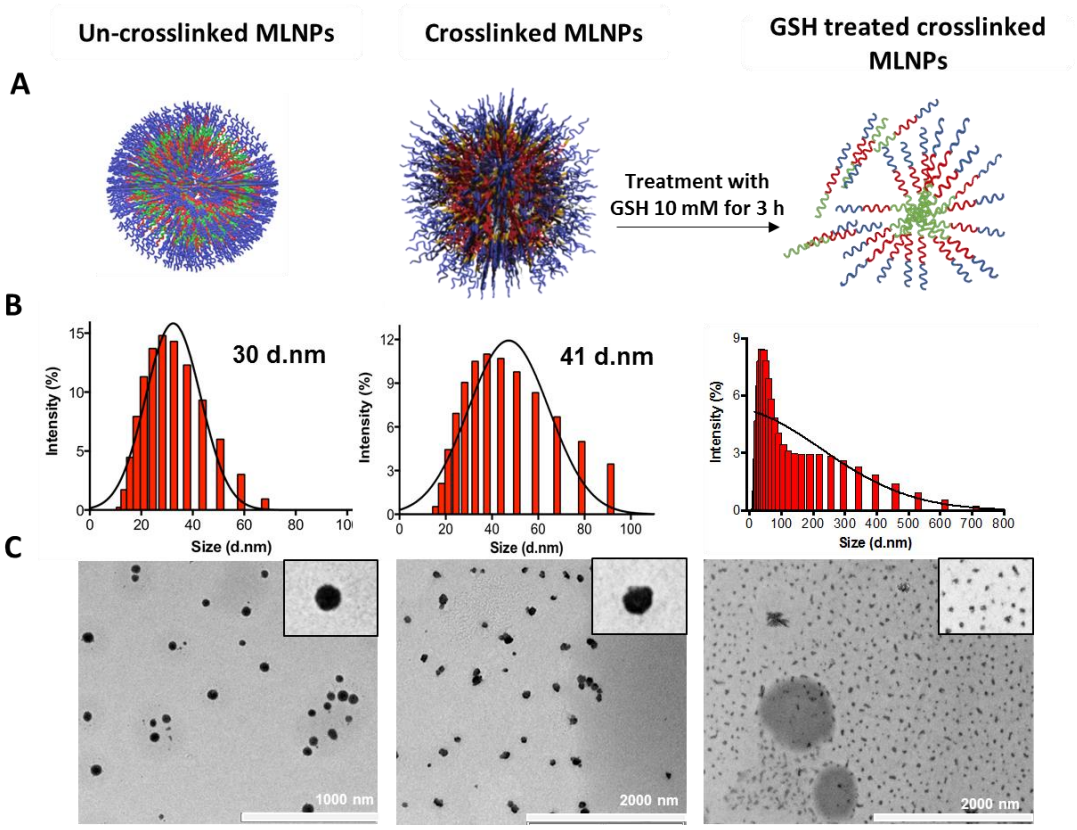

Figure 3 (A) Showing scheme of un-crosslinked MLNPs with free N_3 groups, core crosslinked MLNPs with redox responsive group and crosslinked MLNPs exposed to GSH 10 mM. (B) Size distribution (DLS) of empty crosslinked, un-crosslinked MLNPs and DLS of the redox responsive crosslinked MLNPs after the treatment with glutathione (GSH) 10 mM for 3 hours. Size was based on intensity measured by DLS (n=3). (C) Morphology of the MLNPs (un-crosslinked, crosslinked and crosslinked after treatment with GSH) by transmission electron microscopy. Scale bar 1000 (left), 2000 nm (centre) and 2000 nm (right).

As shown in Figure 3, redox-responsive crosslinked MLNPs were exposed to 10 mM of GSH for 3h and the responsiveness of the particles was investigated through the evaluation of the size and morphology before and after the treatment. In addition, to corroborate the hypothesis regarding the accessibility of the disulfide bond placed in the core of the MLNPs, the same investigation was performed for non-responsive crosslinked MLNPs and also, redox-responsive MLNPs obtained with the comparison terpolymer mPEG-b-poly(εCL-co-αN_3εCL). The characterisation data of the

non-responsive linker and terpolymer are shown in SI Figures S17-19. Comparing the copolymers designed in this work, mPEG-b-poly(D,L-LA-co-αN$_3$εCL) and mPEG-b-poly(εCL-co-αN$_3$εCL), D,L-lactide was substituted by ε-caprolactone with both polymers having a similar molar mass (approximately 7 kDa). It is known that PLA is less hydrophobic than PCL, as the latter is a semicrystalline polymer, whereas D,L-PLA is an amorphous polymer due to its monomers being randomly positioned into the polymer chain [27, 28, 46]. When comparing Figures 4 and S19, from the DLS and TEM images it can be noticed that the crosslinked MLNPs prepared using the copolymer mPEG-b-poly(D,L-LA-co-αN$_3$εCL) presented increased responsiveness to GSH than the MLNPs made from mPEG-b-poly(εCL-co-αN$_3$εCL). Regarding non-responsive crosslinked MLNPs, as seen in Figure S19 the particles were not changed in terms of the size or morphology after treatment with GSH. In terms of drug release in the presence of GSH, according to the data showed, it is expected that the non-responsive crosslinked MLNPs, would not show responsiveness to GSH similarly to the un-crosslinked MLNPs, however with better drug retention similarly to the crosslinked MLNPs when exposed to PBS only, as shown in Figure 4.

The results of drug content and encapsulation efficiency are also shown in Table 1, indicating that the crosslinked MLNPs exhibited better encapsulation efficiency and higher drug contents when compared with the un-crosslinked MLNPs.

Table 1 Characterisation data of empty, Cy5-labelled and DTX-loaded un-crosslinked (un-CC) and redox responsive core crosslinked (CC) MLNPs

Formulation	Size (d.nm) ± SD	Zeta potential (mV) ± SD	Drug loading content (%) ± SD	Encapsulation efficiency (%) ± SD
Un-CC MLNPs	31.6 ± 1.0	- 5.4 ± 0.2	NA	NA
CC MLNPs	41.1 ± 0.5	-6.1 ± 0.2	NA	NA
DTX-loaded un-CC MLNPs	42.6 ± 0.5	-6.8 ± 0.3	2.3 ± 0.1	29.5 ± 1.3
DTX-loaded CC MLNPs	55.3 ± 1.2	-7.9 ± 0.5	6.6 ± 0.3	42.8 ± 0.5
Cy5-labelled CC MLNPs	54.5 ± 0.2	-3.4 ± 0.3	NA	NA
Cy5-labelled un-CC MLNPs	60.9 ± 0.2	-3.9 ± 0.1	NA	NA

n = 3 ± SD (standard deviation), NA – not applicable

In vitro drug release study

In order to assess the responsiveness of crosslinked MLNPs to elevated redox environments, DXT-loaded MLNPs were incubated in the presence or absence of the reducing agent glutathione (GSH). The role of GSH in cancer cells is complex but it has been extensively reported that elevated intracellular levels of GSH are related to protection of these cells through drug resistance mechanisms. High levels of GSH have been found in a number of types of cancer cells, including those in triple negative breast cancer, as previously discussed.

HPLC was used to monitor and compare the release kinetics of DTX from crosslinked and un-crosslinked MLNPs using the developed quantification method (Figure S11). As shown in Figure 4A, the DTX-loaded crosslinked MLNPs in PBS (pH 7.4), without the addition of 10 mM of GSH, showed slow and minimal release.

After 30 h of incubation, the cumulative release of DTX from the crosslinked MLNPs reached 21% and no further release occurred beyond 100 hr. In contrast, DTX-loaded crosslinked MLNPs exposed to PBS containing 10 mM of GSH showed a much faster and greater cumulative DTX release. In the first 10 hours, the crosslinked MLNPs released more than 60% of DTX and after 40 h the cumulative release was almost 100%, as shown in Figure 4A. The release of DTX from the un-crosslinked MLNPs was faster and to a greater extent in comparison to the DTX-loaded crosslinked MLNPs exposed to PBS only.

However, cumulative DTX release from the un-crosslinked MLNPs, in the presence or absence of 10 mM of GSH (Figure 4A-B) was incomplete after 100 hr and significantly less than from the crosslinked MLNPs after addition of GSH. These findings showed that crosslinked MLNPs were able to retain the drug for prolonged times in PBS (pH 7.4) compared to their un-crosslinked counterparts, but that the crosslinked MLNPs were sufficiently sensitive to reducing environments that they were able to release their full drug cargo under these conditions. The data also suggest that carrying out the bis(azide)-bis(alkyne) crosslinking reaction in the presence of DTX fixed the internal structure of the MLNPs and the location of the drug molecules in a different manner to that occurring in the un-crosslinked MLNPs. It is likely that much of the cross-linking occurred in the 'outer core' of the MLNPs, owing to limited diffusion of $CuSO_4$ into the more hydrophobic regions of the block co-polymer, thus localising DTX nearer the solvent accessible regions. In turn, this would allow the drug molecules to escape more readily from the cross-linked MLNPs on

addition of GSH compared to the case for DTX entrapped more deeply in the cores of the un-crosslinked MLNPs.

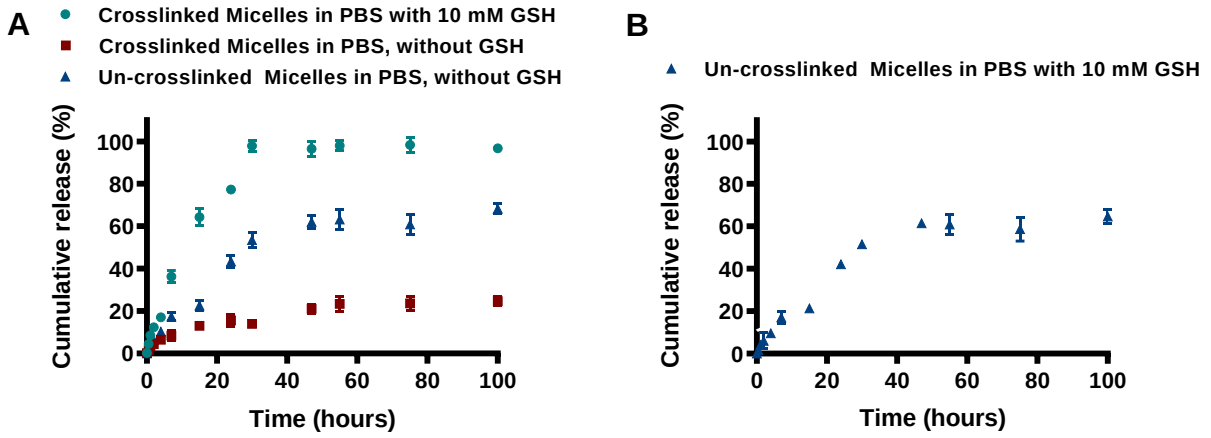

Figure 4 (A) Analysis of docetaxel (DTX) release from DTX-loaded crosslinked MLNPs with and without 10 mM of GSH, to mimic a redox and non-redox environment, and DTX-loaded un-crosslinked MLNPs in PBS without GSH (B) Analysis of docetaxel (DTX) release from DTX-loaded un-crosslinked MLNPs with 10 mM of GSH. DTX was quantified by HPLC and each point represents mean ± SD, n=3. (Statistical analysis is shown in Figure S15 *p < 0.05, **p < 0.01, two-way ANOVA with Tukey's post-test).

Metabolic activity/ cytotoxicity analysis

The metabolic activities of the cells treated with both crosslinked and un-crosslinked empty MLNPs were assessed in two different breast cancer cells lines, MCF7, MDA-MB-231 and in MCF10A, a non-cancerous mammary cell line, as shown in Figure 5. Cells were exposed to different concentrations of MLNPs for 24 h and results demonstrated that both crosslinked and un-crosslinked MLNPs did not show *in vitro* cytotoxicity under the tested conditions. As apparent from Figure 5, the metabolic activity of the cells in the presence of MLNPs was always at least

80% of negative controls for all the cell lines tested. The metabolic activity results were similar to those reported for other copolymer MLNPs based on PLA and PCL as hydrophobic blocks and PEG as a hydrophilic shell, and also with crosslinked micellar formulation using PCL [47].

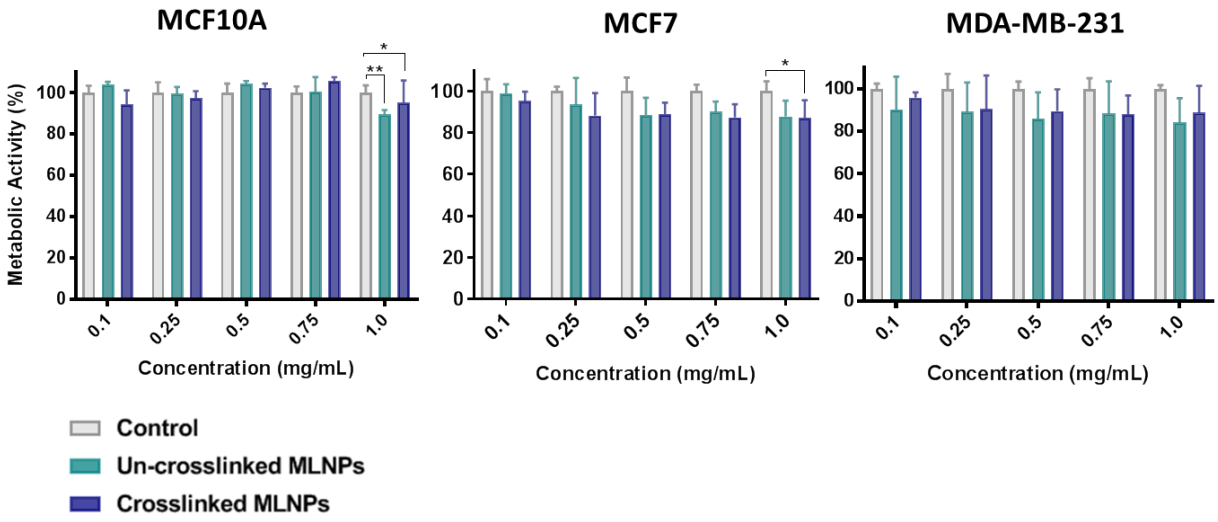

Figure 5 Metabolic activities of cells incubated with crosslinked and un-crosslinked MLNPs (MTS assay). Two breast cancer cell lines and a non-cancerous human breast epithelial cell line MCF10A were used: MCF7, MDA-MB-231 and MCF10A. Error bars show standard deviation (n=5). (*$p < 0.05$, **$p < 0.01$, two-way ANOVA with Tukey's post-test).

The cytotoxicity of DTX-loaded crosslinked and un-crosslinked MLNPs was also assessed by MTS assays in MDA-MB-231 triple negative breast cancer cells, MCF7 breast cancer cells and normal MCF10A mammary breast cells (Figure 6). Before assessing the *in vitro* efficacy of the DTX-loaded MLNPs, the intracellular GSH levels were evaluated using a luminescent-based assay in the mentioned cell lines, as shown in Figure 6A. The results show that MCF7 cells presented the highest levels of intracellular GSH, followed by the MDA-MB-231 and the non-cancerous mammary cells which corroborates with previous reports [48, 49]. It should be noted that MCF7 cells are from an immortalised human estrogen-positive breast cancer cell line. However, when

considering patient-derived breast tumours, correlations between progesterone or estrogen receptor levels with high levels of GSH have not been reported. It has been shown that hormone-positive primary breast tumours tend not to present GSH as a marker of malignancy, in contrast to triple negative breast cancer subtypes [11, 50, 51]. In this context, taking into account that breast cancer is a very heterogeneous disease, the existing in vitro models are not always able to mimic human breast tumours. Thus while the results in Figure 6A indicate that the MCF7 cells exhibited high GSH content, it is likely that this breast cancer cell line might not be representative of true human breast cancers for the specific aspect investigated. As discussed elsewhere [52, 53], although presenting limitations, when immortalised breast cancer cells are used towards the appropriate investigations, they can be powerful tools for the understanding the clinical aspects of breast cancer. Therefore, in order to investigate the responsiveness and efficacy of the DTX-loaded crosslinked MLNPs, all three cell lines were treated with the MLNPs and free docetaxel and the results are shown in Figure 6B-D.

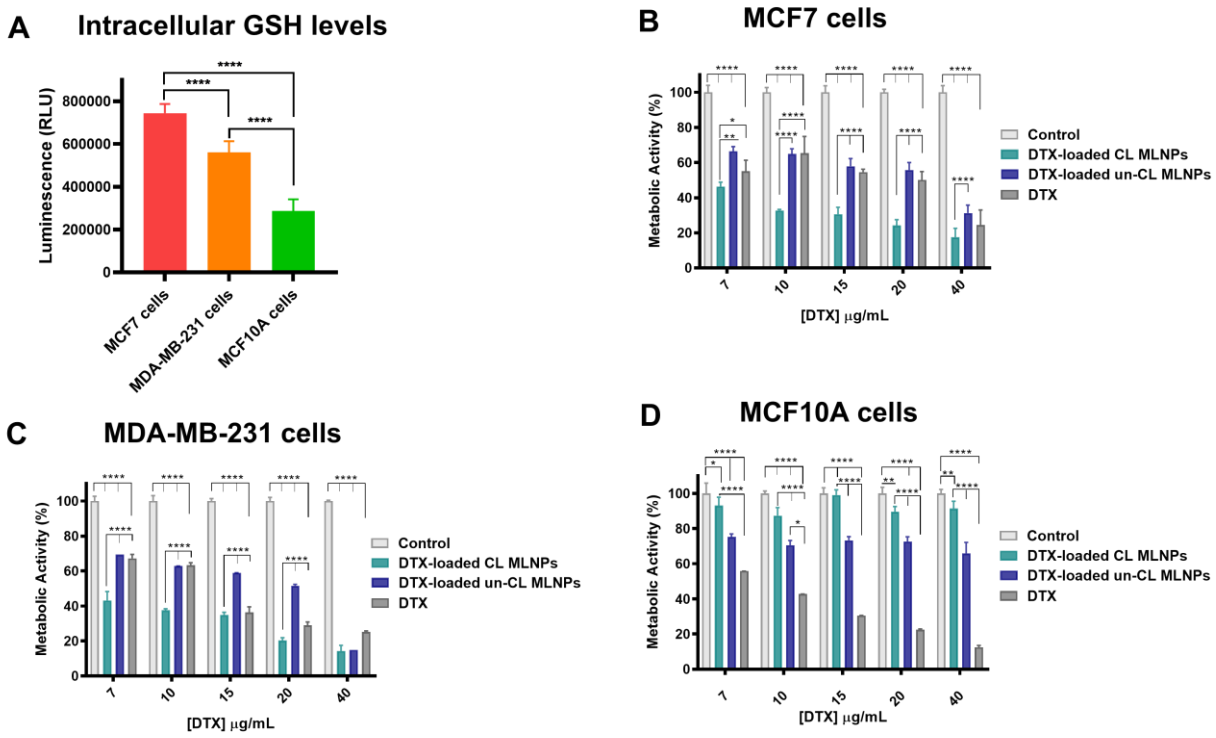

Figure 6 (A) Intracellular GSH levels of MCF7, MDA-MB-231 and MCF10A cells assessed by GSH-Glo™ Glutathione Assay. Cell viability of DTX-loaded crosslinked, un-crosslinked MLNPs and free DTX (MTS assay) of (B) MCF7, (C) MDA-MB-23 and MCF10A cells. Error bars show standard deviation (n=5). (*$p < 0.05$, **$p < 0.01$, ****$p < 0.0001$ two-way ANOVA with Tukey's post-test).

According to Figure 6B-D, the metabolic activity of the MCF7 cells treated with DTX-loaded crosslinked MLNPs was significantly lower than that of the cells treated with un-crosslinked MLNPs and free DTX for all the concentrations tested from 7 to 40 µg/mL of DTX. For the MDA-MB-231, there were significant differences between the treatments up to 40 µg/mL of DTX, but none at the highest concentration. This was likely due to a maximum inhibition of cell metabolic activity at this high concentration of drug. For the concentrations from 7 to 20 µg/mL the DTX-loaded crosslinked MLNPs were also more effective than un-crosslinked MLNPs and free DTX. Since both polymer-only formulations did not affect MCF7 and MDA-MB-231 cell activity, the

high cytotoxicity of the drug-loaded crosslinked MLNPs can be attributed to the enhanced intracellular delivery of DTX and the fact that the stimuli-responsive MLNPs may enhance the release of DTX due to the increased glutathione levels in the triple negative and breast cancer cells, as shown in Figure 6A [54].

To corroborate with the hypothesis that the higher *in vitro* efficacy of the crosslinked MLNPs can be attributed to the increased intracellular glutathione levels of the breast cancer cells, the efficacy of the formulations and free DTX was also investigated in the healthy mammary epithelial cell line, MCF10A. As shown in Figure 6D, the DTX-loaded crosslinked MLNPs were significantly less cytotoxic than the un-crosslinked MLNPs and free DTX. The free DTX presented the highest toxicity levels against the healthy cells, showing a lack of selectivity in between normal and cancer cells. These findings suggest the importance of the development of more clinically relevant drug delivery systems which can result in more effective treatment with fewer side effects for patients, especially for breast cancers where altered redox states may be present within their tumours.

Cell uptake studies in TNBC monolayers (2D) and spheroids (3D)

2D monolayers of TNBC cells

The *in vitro* uptake of Cy5-labelled crosslinked and un-crosslinked MLNPs in 2D monolayers of TNBC was investigated using flow cytometry and confocal microscopy.

Flow cytometry was used to evaluate if the uptake was dependent on the micelle concentration. Therefore, cells were incubated with various concentrations (from 10 µg/mL to 150 µg/mL) of MLNPs for 4 h. Figure 7A and B shows the FACS histograms of evaluated concentrations of crosslinked and un-crosslinked MLNPs. With increasing concentration of MLNPs incubated with

the cells, there were increased detected fluorescence intensities, suggesting that more MLNPs were internalised per cell, or that more cells were internalising labelled MLNPs compared to the negative control (unexposed cells). Figure 7C indicates the difference in the uptake of Cy5-labelled crosslinked and un-crosslinked MLNPs according to the mean fluorescence intensity (MFI) calculated using Kaluza 1.5 software, and these results demonstrated that Cy5-labelled crosslinked MLNPs were internalised to a greater extent than the un-crosslinked MLNPs in 2D monolayers. These results suggest that crosslinking the micelle-core did not prejudice the cellular uptake of the MLNPs into the TNBC cells. The higher cellular uptake of the Cy5-labelled crosslinked MLNPs compared to the un-crosslinked counterparts can be correlated to the size of the MLNPs as shown in Table 1. The empty and DTX-loaded un-crosslinked MLNPs are smaller in size when compared to the crosslinked MLNPs, however, the opposite is observed when comparing the Cy5-labelled formulations. The covalent incorporation of the dye into the polymer backbone seems to have played a role on the cellular uptake of the MLNPs and this can be correlated to the fact that the crosslinked MLNPs possibly have the ability to allow the hydrophobic dyes to organise in a more tightly packed manner in the covalently linked core of the micelles in comparison to the un-crosslinked MLNPs [55].

The intracellular uptake of Cy5-labelled crosslinked and un-crosslinked MLNPs was also assessed by confocal microscopy. MDA-MB-231 cells were exposed to MLNPs at the concentration of 50 µg/mL for 4 h and analysed, as shown in Figure 7D-K. Figure 7D-G shows that crosslinked MLNPs were internalised by the triple negative breast cancer cells. In Figure 7H-K it can be observed that un-crosslinked MLNPs were also taken up by the cells, but this was to a lower extent than the crosslinked MLNPs, which corroborates with the FACS data discussed above. As can be observed in Figure 7 (D-K), Cy5 signals from the crosslinked MLNPs seemed

to be distributed in both the cell membranes (green, stained by CellMask™ green) and also in the cytoplasm, whereas the un-crosslinked micelles appeared to be more located in the cell membranes only in comparison to crosslinked MLNPs. Nevertheless, both formulations were efficiently internalised, as shown in Figure 7.

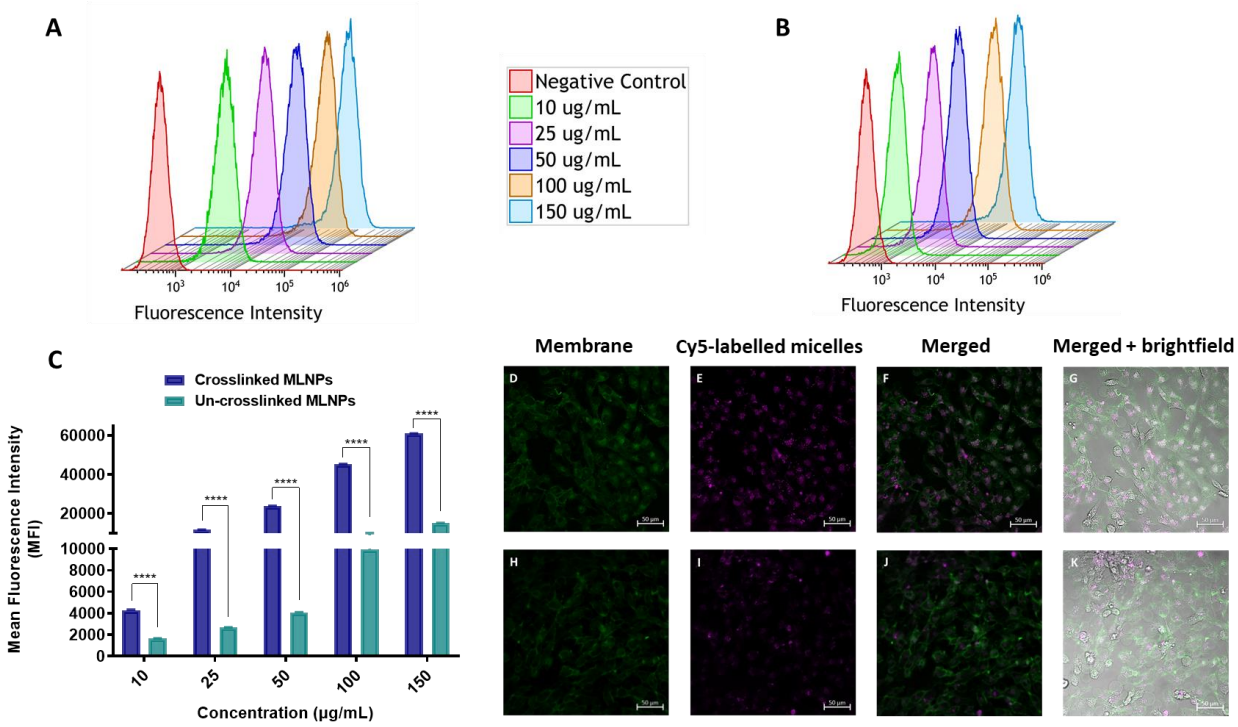

Figure 7 Cellular uptake of Cy5-labelled crosslinked and un-crosslinked MLNPs by MDA-MB-231 breast cancer cells after 4 h of incubation. (A,B) FACS uptake histograms for crosslinked (left) and un-crosslinked (right) MLNPs show uptake is dependent on the concentration of the MLNPs (C) Quantification of MFI with concentration of the Cy5-labelled crosslinked and un-crosslinked MLNPs. Data are representative of three experiments. *P < 0.05, t-test. Confocal microscopy images of MDA-MB-231 breast cancer cells after 4 h of incubation with Cy5-labelled crosslinked and un-crosslinked MLNPs. (D,H) – Green channel: showing the green fluorescence of CellMask green plasma membrane stain. (E,I) – Red channel: Cy5-labelled crosslinked MLNPs and un-crosslinked MLNPs. (F,J-G,K) – Merged: superimposition of all channels and brightfield – Scale bar 50 µm.

3D multicellular spheroids of TNBC cells

The uptake of Cy5-labelled MLNPs was assessed in 3D multicellular tumour spheroids of MDA-MB-231 cells using FACS and confocal microscopy. Results and discussion are shown in the Supportive Information and in Figure S12.

In addition to the assessment of the Cy5-labelled MLNPs uptake in a TNBC 3D spheroid monoculture model, the uptake was also investigated in a co-culture 3D model consisting of MDA-MB-231 and cancer-associated fibroblasts transfected with GFP. The uptake was assessed by FACS and images of the spheroids were also obtained with a confocal microscope as shown in Figure 8.

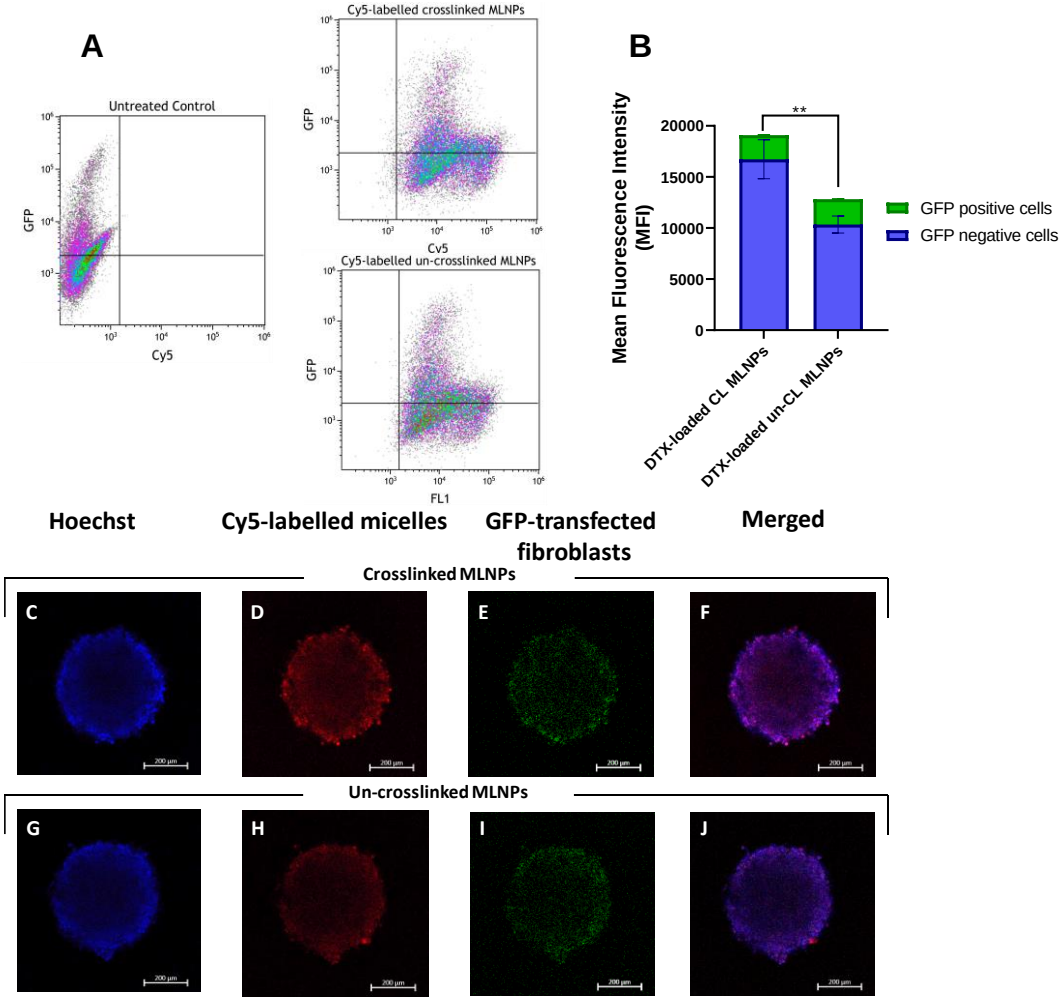

Figure 8 - Cellular uptake of Cy5-labelled crosslinked and un-crosslinked MLNPs by spheroids of MDA-MB-231 TNBC cells and cancer-associated fibroblasts (CAFs) (2000:2000) after 5 h of incubation. (A) FACS histograms showing the population of cells untreated and treated with Cy5-labelled crosslinked and un-crosslinked MLNPs (C) MFI of the Cy5 positive cells distinguishing GFP positive cells (CAFs) and GFP negative cells (MDA-MB-231s). Data are representative of three experiments. (*$p < 0.05$, **$p < 0.01$, ****$p < 0.0001$ two-way ANOVA with Tukey's post-test). Confocal microscopy images of spheroids of MDA-MB-231 TNBC cells and cancer-associated fibroblast after 5 h of incubation with Cy5-labelled crosslinked and un-crosslinked MLNPs. (C,G) – Blue channel: showing nuclei stained with Hoechst. (D,H) – Red channel: Cy5-labelled crosslinked MLNPs and un-crosslinked MLNPs. (E,I) GPF-transfected CAFs cells (F,J) – Merged: superimposition of all channels – Scale bar 200 μm.

Figure 8A,B shows the population of cells untreated (negative control) and cells treated with Cy5-labelled crosslinked and un-crosslinked MLNP. Cy5 positive cells are in the top (CAFs) and bottom right (MDA-MB-231) of the FACS histograms. In Figure 8B is presented the MFI of the Cy5-positive cells encompassing MDA-MB-231 cells and CAFs transfected with GFP. As can be observed, overall the Cy5-labelled crosslinked MLNP were internalised to a greater extent than the un-crosslinked MLNPs in the co-culture 3D spheroids. When distinguishing the cell populations, it is possible to observe that the uptake of the crosslinked MLNPs was higher due to the extended uptake into the triple negative breast cancer cells, MDA-MB-231. Regarding the uptake in CAFs, there was no difference in the MFI values for the crosslinked and un-crosslinked MLNPs.

In Figure 8 (C,J) are shown the results of the uptake assessed by confocal microscopy. Spheroids nuclei were also stained with Hoechst 33342 dye at concentration of 1 μg/mL (50 μL) for 30 minutes. The Cy5-labelled MLNPs penetrated within the spheroids as shown in Figure 8 D,H and in E,I is presented the CAFs transfected with GFP. Finally, the merged images of the channels are

shown in Figure 8 F,J. The fluorescence images corroborate with the FACS data as they demonstrate that both Cy5-labelled MLNPs were taken up by the spheroids, however, the crosslinked MLNPs seem to have been taken up to a greater extent when compared with the un-crosslinked MLNPs.

Comparing Figures 8 and S12, it is noticeable that the addition of CAFs in the 3D spheroids of TNBC cells MDA-MB-231 made the resultant spheroids more compact and thus more relevant as a biological *in vitro* model to mimic TNBC tumours than the monocultures. The addition of fibroblasts in 3D spheroid models has been reported to increase the resistance, promote the modification of signalling pathways, contribute to extracellular matrix environment and promotes cell migration and invasion,[56, 57] and thus the results in the co-culture model in which the cross-linked MLNPs penetrated to the greatest extent were indicative of the promise of this formulation.

3D cell culture is notably more reliable in mimicking the cellular microenvironment *in vivo [58]* and the obtained results are closer to what is expected from the behaviour of nanoparticles in the *in vivo* environment.

Efficacy of MLNPs and free docetaxel in 2D and 3D cell culture

Apoptosis assays in 2D monolayers

Cells were treated with free DTX, DTX-loaded crosslinked and un-crosslinked MLNPs for 24 h. After the specified incubation time, an annexin-V/PI assay was used to discriminate between viable, apoptotic and dead cells using flow cytometry. Three different controls were prepared as shown in Figure 9A. It shows the controls used for observing the basal level of apoptosis, and also the autofluorescence of MDA-MB-231 cells. Figure 9B shows cell populations treated with free DTX and DTX-loaded MLNPs. Live cells which were negative for annexin-V and PI are depicted

in quadrant 3 (Q3). Early apoptotic cells that are positive for annexin-V are located in Q4. Double-positive cells (annexin-V and PI positive), which are considered to be cells in the late stages of apoptosis are shown in Q2, while, Q1 shows necrotic cells that are positive only for PI.

The proportions (%) of different cell populations in each stage are presented in Figure 9C, compared to controls in Figure 9A, considering the basal level of apoptosis and the autofluorescence of cells (negative control). Cells exposed to crosslinked MLNPs were more apoptotic (considering early and late apoptosis) to a level of 31%, followed by un-crosslinked MLNPs (25%) and free DTX (23%) of apoptotic cells. DTX is a microtubule-disruptive apoptotic drug and as shown in Figure 9A-C, DTX-loaded crosslinked MLNPs increased the DTX-induced apoptosis in comparison to the un-crosslinked MLNPs and also, to the free drug.

Caspase activity was also assessed in the MDA-MB-231 cells treated for 24 h with free drug, DTX-loaded crosslinked and un-crosslinked MLNPs using the CellEvent^{TM} caspase-3/7 green detection reagent combined with SYTOX^{TM} AADvanced red. Thus, in this assay apoptotic cells with activated caspase 3/7 were discriminated from necrotic cells using flow cytometry. The distribution of cell populations exposed to free DTX and DTX-loaded MLNPs is shown in Figure 9D-E. In Q3 are the viable cells which are negative for CellEvent^{TM} Caspase 3/7 and SYTOX^{TM} red, whereas Q4 shows apoptotic cells which are positive for CellEvent^{TM} Caspase 3/7. Necrotic cells (Q2) are positive for SYTOX^{TM} red and for CellEvent^{TM} Caspase 3/7.

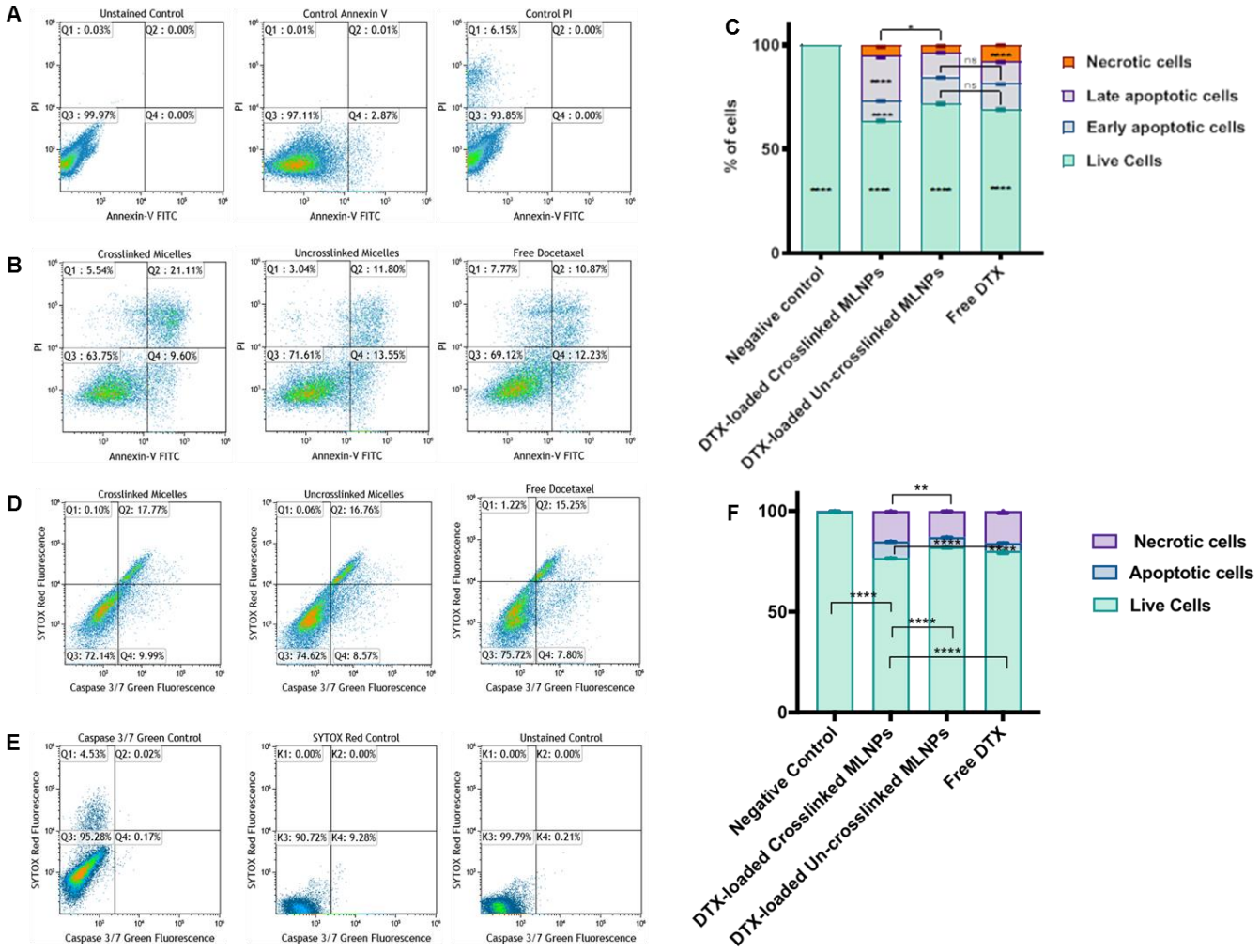

Figure 9 Apoptosis assays annexin-V/ PI and caspase 3/7 and Sytox assessed for the MDA-MB-231 cells treated with DTX-loaded crosslinked and un-crosslinked MLNPs (A) Controls in the panels showing unstained MDA-MB-231 breast cancer cells and controls for annexin-V FITC and PI. (B) MDA-MB-231 breast cancer cells stained with annexin-V FITC and PI, following treatment with crosslinked and un-crosslinked MLNPs encapsulated with DTX and free DTX for 24 h. Samples were analysed by flow cytometry. (C) Showing the proportion (%) of different cell populations after treatment with crosslinked, un-crosslinked MLNPs and free DTX using annexin/PI assay. (D) Controls in the panels showing unstained MDA-MB-231 breast cancer cells and controls for CellEvent Caspase 3/7 and Sytox. (E) MDA-MB-231 triple negative breast cancer cells were treated with crosslinked and un-crosslinked MLNPs encapsulated with DTX and free DTX for 24 h. Samples were labeled with the CellEvent Caspase 3/7 and Sytox red and

analysed by flow cytometry. (F) Cells with caspase-3/7 activation after treatment with crosslinked, un-crosslinked MLNPs and free DTX.

All treatments promoted activation of caspase-3/7 in MDA-MB-231 cells, but cells treated with crosslinked MLNPs had a higher percentage caspase-3/7 activation in comparison to the cells treated with un-crosslinked MLNPs and free DTX (Figure 9F).

Live/Dead assay in 3D spheroids

The efficacy of the DTX-loaded crosslinked and un-crosslinked MLNPs and free DTX in 3D spheroids was assessed by a live/dead staining assay using calcein-AM and ethidium homodimer-1 (EthD-1). After seeding the cells (4000 cells per well), the spheroids were formed within 3 days and were exposed to DTX-loaded crosslinked and un-crosslinked MLNPs and free DTX for 24 h. Spheroids were washed with PBS and subsequently stained with 2 μM of calcein AM and 4 μM of EthD-1 solutions and incubated for 1 h at room temperature. Afterwards, spheroids were carefully washed with PBS and fixed with 4% paraformaldehyde solution for confocal microscopy analysis, or disintegrated prior to plate reader-based quantitative analysis.

As seen in Figure 10, the green fluorescent cells in the spheroids are live cells which present ubiquitous intracellular esterase activity, allowing the nonfluorescent cell-permeant calcein AM to be converted to the highly fluorescent calcein inside these cells. Dead cells displayed red fluorescence due to membrane damage which allowed the penetration of EthD-1 within the cells.

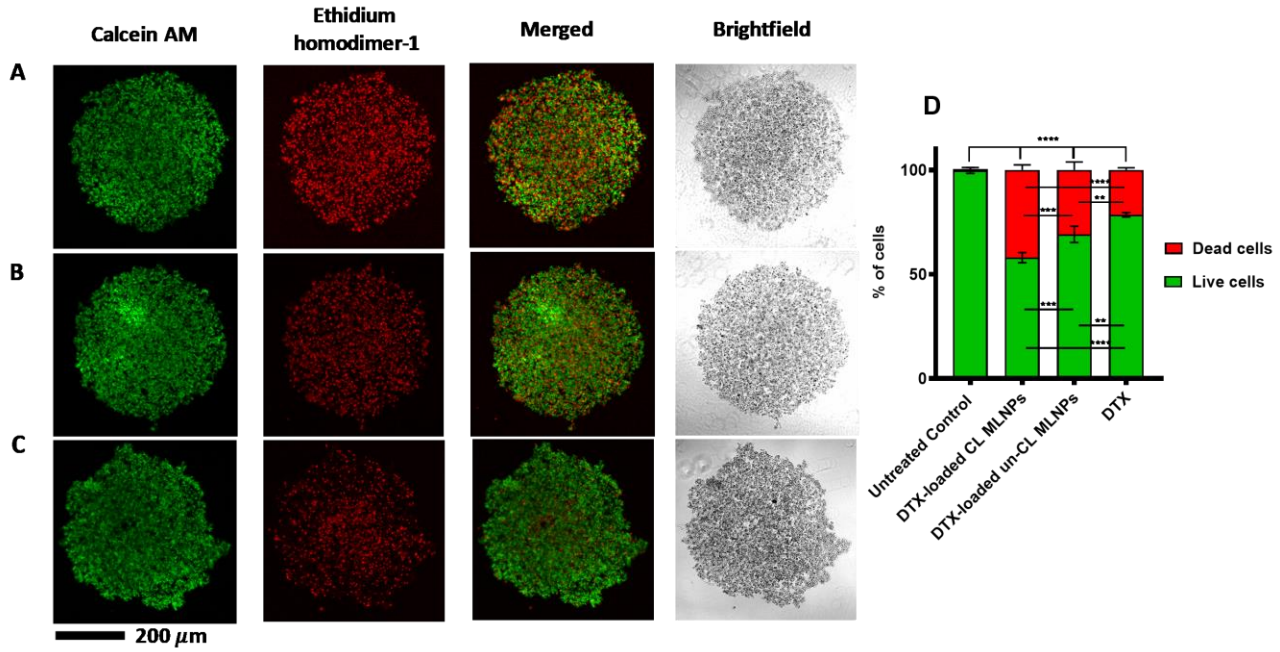

Figure 10 Live/Dead spheroid staining using calcein AM (live cells) and ethidium homodimer-1 (dead cells). Spheroids were treated (24h) with DTX-loaded crosslinked (A), DTX-loaded un-crosslinked MLNPs (B) and free Docetaxel (DTX) (C), at the concentration of 7 μg/mL of DTX. Spheroids were imaged using confocal microscopy. (D) Quantitative data of the live/dead spheroids staining obtained by quantification of the fluorescence intensity.

In Figure 10-AC is shown the confocal images of the live and dead cells within the spheroids after treatment with DTX-loaded crosslinked and un-crosslinked MLNPs and free DTX. Figure 10C is shown the quantitative data obtained by reading the plates containing the disintegrated spheroids using a fluorescence multi-well plate reader. As the results indicate, the spheroid treated with DTX-loaded crosslinked MLNP induced the highest amount of TNBC cell death (red cells) in comparison to the spheroids treated with DTX-loaded un-crosslinked MNLP and free DTX. This result showed that the DTX-loaded crosslinked MLNPs had a superior efficacy even in more complex *in vitro* model (3D spheroids) which present higher innate resistance to drug treatments

[59]. Images of negative control (untreated spheroid) and positive control (spheroid treated with 12% of DMSO) are shown in Figure S13.

CONCLUSIONS

In summary, we have designed DTX-loaded redox-responsive crosslinked MLNPs as potential TNBC therapeutics, using a PEG-poly(lactide-co-caprolactone) terpolymer functionalised such that the degradable linkers were placed in the caprolactone units to modulate accessibility to TNBC cellular reductants. The crosslinked MLNPs exhibited high uptake in TNBC 2D monolayers and also in 3D multicellular spheroid models, monoculture and in a relevant co-culture of TNBC cells with cancer-associated fibroblasts. The reducible-responsive crosslinked MLNPs released higher amounts of drug under redox conditions than the non-reducoble analogues. It was shown that the DTX-loaded reducible crosslinked MLNPs displayed higher cytotoxicity against breast cancer cell lines (including TNBC) with high intracellular amounts of GSH compared to the un-crosslinked MLNPs. TNBC cells treated with DTX-loaded crosslinked MLNPs also showed increased caspase-3/7 activation. In addition, the levels of early and late apoptosis combined were also higher in TNBC cells exposed to the DTX-loaded crosslinked formulations. Regarding efficacy against 3D tumour spheroids, DTX-loaded crosslinked MLNP also showed higher activity in comparison to the un-crosslinked counterparts and to free DTX. Overall, the responsive crosslinked MLNPs were demonstrated to be more effective across multiple assays than the non cross-linked analogues and the free drug. These data together suggest that MLNPs might be a promising treatment for future applications in triple negative breast cancer. However, it will be necessary to demonstrate that the MLNPs are sufficiently stable to circulate following systemic injection, and it is likely that some form of targeting will be needed to enable the polymers to penetrate into tumour tissue

preferentially compared to healthy regions. This might be achieved by addition of ligands at the surface of the micelles which could bind to over-expressed receptors, but as this approach has had limited success in many cases, it might also be necessary to utilise external stimuli such as ultrasound or local tissue heating to enhance permeability within the tumour. Therefore, given the encouraging results obtained from the clinically relevant 3D models, experiments to assess the *in vivo* efficacy in a tumour-bearing model of TNBC will be the next step to investigate further the potential of these nanoformulations.

Corresponding Authors

E-mail: Cameron.alexander@nottingham.ac.uk

Author Contributions

The manuscript was written through contributions of all authors. All authors have given approval to the final version of the manuscript.

Funding Sources

EPSRC for funding [EP/N006615/1] EPSRC Programme Grant for Next Generation Biomaterials Discovery" and grants [EP/H005625/1, EP/N03371X/1], the Royal Society [Wolfson Research Merit Award WM150086 to CA]. CAPES (Coordenação de Aperfeiçoamento de Pessoal de Nível Superior – Brazil) for the PhD scholarships (PM and CM). The European Commission, Education, Audiovisual and Cultural Executive Agency, (EACEA) for an Erasmus Mundus grant to MG (NanoFar Joint Doctoral Program).

ACKNOWLEDGMENTS

We thank EPSRC for funding [Grants EP/N006615/1, EP/H005625/1, EP/N03371X/1, EP/N006615/1], the Royal Society [Wolfson Research Merit Award WM150086 to CA], and CAPES (Coordenação de Aperfeiçoamento de Pessoal de Nível Superior – Brazil) for the PhD scholarships (PM and CM). We also thank the European Commission, Education, Audiovisual and Cultural Executive Agency, (EACEA) for an Erasmus Mundus grant to MG (NanoFar Joint Doctoral Program). We acknowledge Dr. Rory de Brito and Dr. David Onion for expert assistance in FACS data analysis. We also thank Carol Turrill for outstanding administrative support and Barbara Rampersad and Paul Cooling for expert technical support. The Nanoscale & Macroscale Research Center (NMRC) is acknowledged for providing the facilities for TEM analysis.

ABBREVIATIONS

CAFs, cancer-associated fibroblasts; DTX, docetaxel; DLS, dynamic light scattering, MLNPs, micelle-like nanoparticles; GSH, glutathione; PBS, Phosphate buffered saline; TEM, transmission electron microscopy; TNBC, triple negative breast cancer;

REFERENCES

[1] P. Boyle, Triple-negative breast cancer: epidemiological considerations and recommendations, Ann Oncol 23 Suppl 6 (2012) vi7-12.
[2] G. Stockmans, K. Deraedt, H. Wildiers, P. Moerman, R. Paridaens, Triple-negative breast cancer, Curr Opin Oncol 20(6) (2008) 614-20.
[3] M. De Laurentiis, D. Cianniello, R. Caputo, B. Stanzione, G. Arpino, S. Cinieri, V. Lorusso, S. De Placido, Treatment of triple negative breast cancer (TNBC): current options and future perspectives, Cancer Treat Rev 36 Suppl 3 (2010) S80-6.
[4] C.M. Perou, T. Sorlie, M.B. Eisen, M. van de Rijn, S.S. Jeffrey, C.A. Rees, J.R. Pollack, D.T. Ross, H. Johnsen, L.A. Akslen, O. Fluge, A. Pergamenschikov, C. Williams, S.X. Zhu, P.E. Lonning, A.L. Borresen-Dale, P.O. Brown, D. Botstein, Molecular portraits of human breast tumours, Nature 406(6797) (2000) 747-52.
[5] J. Crown, J. O'Shaughnessy, G. Gullo, Emerging targeted therapies in triple-negative breast cancer, Ann Oncol 23 Suppl 6 (2012) vi56-65.
[6] B.P. Schneider, E.P. Winer, W.D. Foulkes, J. Garber, C.M. Perou, A. Richardson, G.W. Sledge, L.A. Carey, Triple-negative breast cancer: risk factors to potential targets, Clin Cancer Res 14(24) (2008) 8010-8.

[7] H. Gelderblom, J. Verweij, K. Nooter, A. Sparreboom, Cremophor EL: the drawbacks and advantages of vehicle selection for drug formulation, Eur J Cancer 37(13) (2001) 1590-8.
[8] F. Andre, C.C. Zielinski, Optimal strategies for the treatment of metastatic triple-negative breast cancer with currently approved agents, Ann Oncol 23 Suppl 6 (2012) vi46-51.
[9] H. Lu, D. Samanta, L. Xiang, H. Zhang, H. Hu, I. Chen, J.W. Bullen, G.L. Semenza, Chemotherapy triggers HIF-1-dependent glutathione synthesis and copper chelation that induces the breast cancer stem cell phenotype, Proceedings of the National Academy of Sciences of the United States of America 112(33) (2015) E4600-9.
[10] T. Miran, A.T.J. Vogg, N. Drude, F.M. Mottaghy, A. Morgenroth, Modulation of glutathione promotes apoptosis in triple-negative breast cancer cells, FASEB J 32(5) (2018) 2803-2813.
[11] A. Beatty, L.S. Fink, T. Singh, A. Strigun, E. Peter, C.M. Ferrer, E. Nicolas, K.Q. Cai, T.P. Moran, M.J. Reginato, U. Rennefahrt, J.R. Peterson, Metabolite Profiling Reveals the Glutathione Biosynthetic Pathway as a Therapeutic Target in Triple-Negative Breast Cancer, Molecular cancer therapeutics 17(1) (2018) 264-275.
[12] H. Yao, G.C. He, S.C. Yan, C. Chen, L.J. Song, T.J. Rosol, X.Y. Deng, Triple-negative breast cancer: is there a treatment on the horizon?, Oncotarget 8(1) (2017) 1913-1924.
[13] D. Peer, J.M. Karp, S. Hong, O.C. Farokhzad, R. Margalit, R. Langer, Nanocarriers as an emerging platform for cancer therapy, Nature nanotechnology 2(12) (2007) 751-60.
[14] X. He, K. Cai, Y. Zhang, Y. Lu, Q. Guo, Y. Zhang, L. Liu, C. Ruan, Q. Chen, X. Chen, C. Li, T. Sun, J. Cheng, C. Jiang, Dimeric Prodrug Self-Delivery Nanoparticles with Enhanced Drug Loading and Bioreduction Responsiveness for Targeted Cancer Therapy, ACS Appl Mater Interfaces 10(46) (2018) 39455-39467.
[15] R.V. Kutty, S.L. Chia, M.I. Setyawati, M.S. Muthu, S.S. Feng, D.T. Leong, In vivo and ex vivo proofs of concept that cetuximab conjugated vitamin E TPGS micelles increases efficacy of delivered docetaxel against triple negative breast cancer, Biomaterials 63 (2015) 58-69.
[16] X. Deng, M. Cao, J. Zhang, K. Hu, Z. Yin, Z. Zhou, X. Xiao, Y. Yang, W. Sheng, Y. Wu, Y. Zeng, Hyaluronic acid-chitosan nanoparticles for co-delivery of MiR-34a and doxorubicin in therapy against triple negative breast cancer, Biomaterials 35(14) (2014) 4333-44.
[17] R. Devulapally, N.M. Sekar, T.V. Sekar, K. Foygel, T.F. Massoud, J.K. Willmann, R. Paulmurugan, Polymer nanoparticles mediated codelivery of antimiR-10b and antimiR-21 for achieving triple negative breast cancer therapy, ACS Nano 9(3) (2015) 2290-302.
[18] S. Mura, J. Nicolas, P. Couvreur, Stimuli-responsive nanocarriers for drug delivery, Nat Mater 12(11) (2013) 991-1003.
[19] G.K. Balendiran, R. Dabur, D. Fraser, The role of glutathione in cancer, Cell Biochem Funct 22(6) (2004) 343-352.
[20] R.R. Perry, J. Mazetta, M. Levin, S.C. Barranco, Glutathione Levels and Variability in Breast-Tumors and Normal Tissue, Cancer 72(3) (1993) 783-787.
[21] S.J. Berger, D. Gosky, E. Zborowska, J.K.V. Willson, N.A. Berger, Sensitive Enzymatic Cycling Assay for Glutathione - Measurements of Glutathione Content and Its Modulation by Buthionine Sulfoximine in-Vivo and in-Vitro in Human Colon-Cancer, Cancer Res 54(15) (1994) 4077-4083.
[22] J.A. Cook, H.I. Pass, S.N. Iype, N. Friedman, W. Degraff, A. Russo, J.B. Mitchell, Cellular Glutathione and Thiol Measurements from Surgically Resected Human Lung-Tumor and Normal Lung-Tissue, Cancer Res 51(16) (1991) 4287-4294.

[23] Y.C. Xia, H. He, X.Y. Liu, D. Hu, L.C. Yin, Y.B. Lu, W.J. Xua, Redox-responsive, core-crosslinked degradable micelles for controlled drug release, Polym Chem-Uk 7(41) (2016) 6330-6339.
[24] C.C. Wang, L.C. Liu, H.L. Cao, W.A. Zhang, Intracellular GSH-activated galactoside photosensitizers for targeted photodynamic therapy and chemotherapy, Biomater Sci-Uk 5(2) (2017) 274-284.
[25] X.B. Zhao, P. Liu, Reduction-Responsive Core-Shell-Corona Micelles Based on Triblock Copolymers: Novel Synthetic Strategy, Characterization, and Application As a Tumor Microenvironment-Responsive Drug Delivery System, Acs Appl Mater Inter 7(1) (2015) 166-174.
[26] C. Conte, F. Mastrotto, V. Taresco, A. Tchoryk, F. Quaglia, S. Stolnik, C. Alexander, Enhanced uptake in 2D-and 3D-lung cancer cell models of redox responsive PEGylated nanoparticles with sensitivity to reducing extra- and intracellular environments, J Control Release 277 (2018) 126-141.
[27] X. Zhang, X. Peng, S.W. Zhang, 7 - Synthetic biodegradable medical polymers: Polymer blends, in: X. Zhang (Ed.), Science and Principles of Biodegradable and Bioresorbable Medical Polymers, Woodhead Publishing2017, pp. 217-254.
[28] D. Newman, E. Laredo, A. Bello, A. Grillo, J.L. Feijoo, A.J. Müller, Molecular Mobilities in Biodegradable Poly(dl-lactide)/Poly(ε-caprolactone) Blends, Macromolecules 42(14) (2009) 5219-5225.
[29] H. Chen, S. Kim, L. Li, S. Wang, K. Park, J.X. Cheng, Release of hydrophobic molecules from polymer micelles into cell membranes revealed by Forster resonance energy transfer imaging, Proceedings of the National Academy of Sciences of the United States of America 105(18) (2008) 6596-601.
[30] R. Wei, L. Cheng, M. Zheng, R. Cheng, F. Meng, C. Deng, Z. Zhong, Reduction-responsive disassemblable core-cross-linked micelles based on poly(ethylene glycol)-b-poly(N-2-hydroxypropyl methacrylamide)-lipoic acid conjugates for triggered intracellular anticancer drug release, Biomacromolecules 13(8) (2012) 2429-38.
[31] L. Zhang, K. Katapodi, T.P. Davis, C. Barner-Kowollik, M.H. Stenzel, Using the reversible addition–fragmentation chain transfer process to synthesize core-crosslinked micelles, Journal of Polymer Science Part A: Polymer Chemistry 44(7) (2006) 2177-2194.
[32] P. Zhang, H. Zhang, W. He, D. Zhao, A. Song, Y. Luan, Disulfide-Linked Amphiphilic Polymer-Docetaxel Conjugates Assembled Redox-Sensitive Micelles for Efficient Antitumor Drug Delivery, Biomacromolecules 17(5) (2016) 1621-32.
[33] A.W. Du, H. Lu, M.H. Stenzel, Core-Cross-Linking Accelerates Antitumor Activities of Paclitaxel-Conjugate Micelles to Prostate Multicellular Tumor Spheroids: A Comparison of 2D and 3D Models, Biomacromolecules 16(5) (2015) 1470-1479.
[34] Q. Hu, C.J. Rijcken, R. Bansal, W.E. Hennink, G. Storm, J. Prakash, Complete regression of breast tumour with a single dose of docetaxel-entrapped core-cross-linked polymeric micelles, Biomaterials 53 (2015) 370-378.
[35] M. Talelli, M. Barz, C.J.F. Rijcken, F. Kiessling, W.E. Hennink, T. Lammers, Core-crosslinked polymeric micelles: Principles, preparation, biomedical applications and clinical translation, Nano Today 10(1) (2015) 93-117.
[36] Kenry, B. Liu, Bio-orthogonal Click Chemistry for In Vivo Bioimaging, Trends in Chemistry 1(8) (2019) 763-778.

[37] J.E. Moses, A.D. Moorhouse, The growing applications of click chemistry, Chemical Society Reviews 36(8) (2007) 1249-1262.
[38] M. Gulfam, T. Matini, P.F. Monteiro, R. Riva, H. Collins, K. Spriggs, S.M. Howdle, C. Jerome, C. Alexander, Bioreducible cross-linked core polymer micelles enhance in vitro activity of methotrexate in breast cancer cells, Biomater Sci 5(3) (2017) 532-550.
[39] S. Lenoir, R. Riva, X. Lou, C. Detrembleur, R. Jérôme, P. Lecomte, Ring-Opening Polymerization of α-Chloro-ε-caprolactone and Chemical Modification of Poly(α-chloro-ε-caprolactone) by Atom Transfer Radical Processes, Macromolecules 37(11) (2004) 4055-4061.
[40] S. Cajot, N. Lautram, C. Passirani, C. Jerome, Design of reversibly core cross-linked micelles sensitive to reductive environment, J Control Release 152(1) (2011) 30-6.
[41] J.H. Saunders, D. Onion, P. Collier, M.S. Dorrington, R.H. Argent, P.A. Clarke, A.M. Reece-Smith, S.L. Parsons, A.M. Grabowska, Individual patient oesophageal cancer 3D models for tailored treatment, Oncotarget 8(15) (2017) 24224-24236.
[42] H.Y. Su, Y.H. Liu, D. Wang, C.Q. Wu, C.C. Xia, Q.Y. Gong, B. Song, H. Ai, Amphiphilic starlike dextran wrapped superparamagnetic iron oxide nanoparticle clsuters as effective magnetic resonance imaging probes, Biomaterials 34(4) (2013) 1193-1203.
[43] S. Acharya, S.K. Sahoo, PLGA nanoparticles containing various anticancer agents and tumour delivery by EPR effect, Adv Drug Deliver Rev 63(3) (2011) 170-183.
[44] S.D. Perrault, C. Walkey, T. Jennings, H.C. Fischer, W.C.W. Chan, Mediating Tumor Targeting Efficiency of Nanoparticles Through Design, Nano Lett 9(5) (2009) 1909-1915.
[45] H. Cabral, Y. Matsumoto, K. Mizuno, Q. Chen, M. Murakami, M. Kimura, Y. Terada, M.R. Kano, K. Miyazono, M. Uesaka, N. Nishiyama, K. Kataoka, Accumulation of sub-100 nm polymeric micelles in poorly permeable tumours depends on size, Nature nanotechnology 6(12) (2011) 815-823.
[46] M.-H. Huang, S. Li, D.W. Hutmacher, J. Coudane, M. Vert, Degradation characteristics of poly(ϵ-caprolactone)-based copolymers and blends, Journal of Applied Polymer Science 102(2) (2006) 1681-1687.
[47] S. Cajot, D. Schol, F. Danhier, V. Preat, M.C.G. De Pauw, C. Jerome, In Vitro Investigations of Smart Drug Delivery Systems Based on Redox-Sensitive Cross-Linked Micelles, Macromol Biosci 13(12) (2013) 1661-1670.
[48] S.S. Syed Alwi, B.E. Cavell, A. Donlevy, G. Packham, Differential induction of apoptosis in human breast cancer cell lines by phenethyl isothiocyanate, a glutathione depleting agent, Cell Stress Chaperones 17(5) (2012) 529-38.
[49] S.H. Cheng, Y.M. Tseng, S.H. Wu, S.M. Tsai, L.Y. Tsai, Whey Protein Concentrate Renders MDA-MB-231 Cells Sensitive to Rapamycin by Altering Cellular Redox State and Activating GSK3beta/mTOR Signaling, Sci Rep 7(1) (2017) 15976.
[50] R.R. Perry, J.A. Mazetta, M. Levin, S.C. Barranco, Glutathione levels and variability in breast tumors and normal tissue, Cancer 72(3) (1993) 783-7.
[51] B.V. Jardim, M.G. Moschetta, C. Leonel, G.B. Gelaleti, V.R. Regiani, L.C. Ferreira, J.R. Lopes, D.A. Zuccari, Glutathione and glutathione peroxidase expression in breast cancer: an immunohistochemical and molecular study, Oncol Rep 30(3) (2013) 1119-28.
[52] T. Vargo-Gogola, J.M. Rosen, Modelling breast cancer: one size does not fit all, Nature Reviews Cancer 7(9) (2007) 659-672.
[53] D.L. Holliday, V. Speirs, Choosing the right cell line for breast cancer research, Breast Cancer Res 13(4) (2011) 215.

[54] R. Cheng, F.H. Meng, C. Deng, H.A. Klok, Z.Y. Zhong, Dual and multi-stimuli responsive polymeric nanoparticles for programmed site-specific drug delivery, Biomaterials 34(14) (2013) 3647-3657.
[55] A. Rajak, C.K. Karan, P. Theato, A. Das, Supramolecularly cross-linked amphiphilic block copolymer assembly by the dipolar interaction of a merocyanine dye, Polym Chem-Uk (2020).
[56] M. Zoetemelk, M. Rausch, D.J. Colin, O. Dormond, P. Nowak-Sliwinska, Short-term 3D culture systems of various complexity for treatment optimization of colorectal carcinoma, Scientific Reports 9(1) (2019) 7103.
[57] L. Li, Y. Lu, Optimizing a 3D Culture System to Study the Interaction between Epithelial Breast Cancer and Its Surrounding Fibroblasts, Journal of Cancer 2 (2011) 458-466.
[58] M. Mirbagheri, V. Adibnia, B.R. Hughes, S.D. Waldman, X. Banquy, D.K. Hwang, Advanced cell culture platforms: a growing quest for emulating natural tissues, Mater Horiz 6(1) (2019) 45-71.
[59] P. Longati, X. Jia, J. Eimer, A. Wagman, M.R. Witt, S. Rehnmark, C. Verbeke, R. Toftgard, M. Lohr, R.L. Heuchel, 3D pancreatic carcinoma spheroids induce a matrix-rich, chemoresistant phenotype offering a better model for drug testing, BMC Cancer 13 (2013) 95.